Structural and functional studies of the RBPJ-SHARP complex reveal conserved corepressor binding site

Zhenyu Yuan[1*], Bradley D. VanderWielen[1*], Benedetto Daniele Giaimo[2], Leiling Pan[3], Courtney E. Collins[1], Aleksandra Turkiewicz[2], Kerstin Hein[2], Franz Oswald[3], Tilman Borggrefe[2] & Rhett A. Kovall[1]

[1]Department of Molecular Genetics, Biochemistry and Microbiology, University of Cincinnati College of Medicine, Cincinnati, Ohio, USA, [2]Institute of Biochemistry, University of Giessen, Giessen, Germany, [3]Department of Internal Medicine I, Center for Internal Medicine, University Medical Center Ulm, 89081 Ulm, Germany. Correspondence should be addressed to RAK, E-mail: kovallra@ucmail.uc.edu

**These authors contributed equally to this work.*

Abstract

The Notch pathway is a conserved signaling mechanism that is essential for cell fate decisions during pre and postnatal development. Dysregulated signaling underlies the pathophysiology of numerous human diseases, most notably T-cell acute lymphoblastic leukemia. Receptor-ligand interactions result in changes in gene expression, which are regulated by the transcription factor CSL. CSL forms a complex with the intracellular domain of the Notch receptor and the transcriptional coactivator Mastermind, which is required to activate transcription of all Notch target genes. CSL can also function as repressor by interacting with corepressor proteins, *e.g.* SHARP in mammals and Hairless in *Drosophila melanogaster*; however, its role as a transcriptional repressor is not well understood. Here we determine the high-resolution structure of RBPJ, the mouse CSL ortholog, bound to the corepressor SHARP and DNA, which reveals a new mode of corepressor binding to CSL and an interesting example for how ligand binding sites evolve in proteins. Based on the structure, we designed and tested a number of mutants in biophysical, biochemical, and cellular assays to characterize the role of RBPJ as a repressor of Notch target genes. Our cellular studies clearly demonstrate that RBPJ mutants that are deficient for binding SHARP are incapable of repressing transcription from genes responsive to Notch signaling. Altogether, our structure-function studies of the RBPJ-SHARP corepressor

complex bound to DNA provide significant insights into the repressor function of RBPJ and identify a new binding pocket on RBPJ that could be targeted for therapeutic benefit.

Introduction

The Notch pathway is a highly conserved cell-to-cell signaling mechanism that is indispensable for cell fate decisions during prenatal development and postnatal tissue homeostasis.[1,2] Dysregulated signaling underlies the pathogenesis of many human diseases, including certain types of cancer, congenital defects, and cardiovascular disease[3]. Given its association with human disease, there have been extensive efforts to identify reagents that pharmaceutically modulate the Notch pathway with most efforts focused on modalities that curtail overactive Notch signaling[4,5]. However, there is a need to identify components in the Notch pathway that when pharmacologically targeted result in upregulated signaling to treat diseases associated with insufficient Notch signaling[3], such as myeloid leukemia, head and neck squamous cell carcinoma, bicuspid aortic valve disease, and Alagille syndrome.

Notch signaling is initiated when Notch receptors on one cell interact with a DSL (Delta, Serrate, Lag-2) ligand on a neighboring cell (Figure 1A)[6]. Extracellular Notch-DSL interactions result in proteolytic cleavage of the receptor, which frees the intracellular domain of Notch (NICD) from the cell membrane, allowing NICD to migrate into the nucleus. Nuclear NICD directly binds the transcription factor CSL [CBF1/RBPJ, Su(H), Lag-1] and the CSL-NICD complex recruits a member of the Mastermind (MAM) family of transcriptional coactivators [Mastermind-like (MAML1-3) in mammals], resulting in the transcriptional activation of Notch target genes (Figure 1A)[7]. CSL can also function as a repressor by interacting with corepressor proteins, such as SHARP [SMRT/HDAC1-associated repressor protein, *also known as* MINT (Msx2-interacting nuclear target) or SPEN (split ends)][8,9], Hairless in *Drosophila melanogaster*[10], FHL1 (Four and a half LIM domains 1, *also known as* KyoT2)[11], L3MBTL3 (lethal 3 malignant

57 brain tumor-like 3)[12], and RITA1 (RBPJ-interacting and tubulin associated)[13,14]. Corepressors
58 are part of large higher order transcriptional repression complexes that contain histone-
59 modifying activity, *e.g.* histone deacetylase or histone demethylase, which convert chromatin
60 into a transcriptionally repressed state (Figure 1A)[7].

61 Crystal structures of Notch transcription complexes have revealed that all CSL proteins
62 contain a conserved structural core composed of three domains termed NTD (N-terminal
63 domain), BTD (β-trefoil domain), and CTD (C-terminal domain) (Figure 1B,C)[15-17]. The NTD and
64 CTD are immunoglobulin (Ig) domains that are structurally similar to the Rel homology region
65 (RHR) of transcription factors, such as NF-κB and NFAT (Nuclear factor of activated T-cells),
66 whereas the fold of the BTD is related to cytokine and growth factor structures, such as
67 Interleukin1 and FGF (Fibroblast Growth Factor)[17]. The NTD and BTD form an electropositive
68 surface that recognizes nucleotides in the major and minor grooves of DNA, respectively[17]. In
69 the transcriptionally active CSL-NICD-MAM ternary complex bound to DNA structure (Figure
70 1B,C), the RAM and ANK domains of NICD bind the BTD and CTD domains of CSL,
71 respectively, and MAM forms an elongated bent helical structure that binds the CTD-ANK
72 interface and the NTD of CSL[15,16]. In addition to the CSL-NICD-MAM activator complex, several
73 CSL-corepressor structures have been determined, including the *Drosophila* corepressor
74 Hairless bound to Su(H) (the fly CSL ortholog)[18], as well as FHL1 and RITA1 bound to RBPJ
75 (mouse/human CSL ortholog)[13,19]. These studies reveal that the binding of Hairless to the CTD
76 of Su(H) produces a large conformational change in CTD[18]; whereas, FHL1 and RITA1 have
77 regions similar to the RAM domain of NICD and bind the BTD of RBPJ in a structurally similar
78 manner[13,19].

79 SHARP is a large multidomain transcriptional coregulator protein that has folded
80 functional domains separated by long regions that are intrinsically disordered. Notably, SHARP
81 has no sequence similarity with any of the previously identified corepressors that bind CSL

82 (Figure 1C). SHARP was originally identified in yeast two-hybrid screens for factors that interact
83 with SMRT/NCoR and the transcription factor MSX2[20,21]. SHARP has traditionally been thought
84 of as a corepressor, because it binds SMRT/NCoR through its C-terminal SPOC domain and
85 represses transcription[9,20,22,23]; however, it has also been shown that through its SPOC domain
86 SHARP can also recruit the KMT2D coactivator complex to Notch target genes[24]. More recently,
87 it has been demonstrated that the N-terminal RRM (RNA recognition motif) domains of SHARP
88 bind the lncRNA Xist and this interaction is important for X chromosome inactivation[25,26].
89 Previously, we defined a region in SHARP that binds RBPJ, termed RBPID (RBPJ-interacting
90 domain, Figure 1C) and showed that RBPJ and SHARP form a high affinity complex[9,27].

91 Here we determine the X-ray structure of the RBPJ-SHARP corepressor complex bound
92 to DNA. We identify structure-based mutants that are essential for RBPJ-mediated repression
93 and characterize these mutants both *in vitro* and in cellular assays. Taken together, our studies
94 reveal the conserved interface of the RBPJ/SHARP corepressor complex, which provides
95 molecular insights into RBPJ repressor function and identify a potential site on RBPJ that could
96 be pharmacologically targeted to upregulate Notch signaling.

97

98 **Results**

99 **Structure determination of the RBPJ/SHARP/DNA complex**

100 In order to determine the X-ray structure of the RBPJ/SHARP corepressor complex bound to
101 DNA, we purified recombinant RBPJ and SHARP proteins from bacteria, corresponding to the
102 structural core of RBPJ (residues 53-474) and the RBPJ-interacting domain (RBPID) of SHARP
103 (residues 2776-2820), formed complexes with a 13mer oligomeric DNA duplex with single-
104 stranded overhangs, containing a single RBPJ binding site, and screened the
105 RBPJ/SHARP/DNA complex for crystallization conditions. While we were able to isolate

106 crystallization conditions for the complex, despite extensive optimization efforts, we were unable
107 to produce diffraction quality crystals amenable for structural analysis. Therefore, we produced
108 an MBP (maltose binding protein) fusion protein with the RBPID of SHARP (MBP-SHARP), *i.e.*
109 fixed-arm carrier approach[28], in which the MBP moiety also has surface entropy reduction
110 mutations engineered into it, in order to identify new crystallization conditions for the
111 RBPJ/MBP-SHARP/DNA complex. This strategy successfully led to crystals that nominally
112 diffract to 2.8 Å resolution and belong to the space group $P2_1$ (a=54.5 Å, b=231.6 Å, c=90.3 Å,
113 and β=99.88°) (Table 1). We demonstrated that our MBP-SHARP construct binds RBPJ
114 similarly as the native SHARP construct, albeit with somewhat weaker affinity (Figure S1B). This
115 is likely due to the close crystal contacts between MBP and RBPJ required for crystallization of
116 the complex. The RBPJ/MBP-SHARP/DNA complex structure was solved by molecular
117 replacement and refined to a final R factor and free R factor of 19.4% and 22.8%, respectively
118 (Table 1).

119 There are two RBPJ-MBP-SHARP/DNA complexes in the asymmetric unit (AU) of the
120 crystals (Figure S1A) that overall are very structurally similar (RMSD 2.28 for 819 cα atoms),
121 with even higher structural correspondence when either MBP (RMSD 0.07 for 297 cα atoms) or
122 RBPJ (RMSD 0.66 for 388 cα atoms) are aligned individually (Figure S1C-E). The largest
123 structural difference between the two complexes in the AU is a poorly ordered linker region in
124 SHARP (Figure S1F), whereby the different conformations are likely influenced by different
125 environments within the crystals. For clarity in subsequent figures, we do not show the MBP
126 moiety and all structural comparisons are performed with chains G & H of RBPJ and SHARP,
127 respectively, as these proteins chains have overall lower temperature factors.

128

129 **Bipartite interaction of SHARP with RBPJ**

130 As shown in Figure 2A-B, SHARP interacts with two distinct surfaces on RBPJ, contacting the
131 CTD and the BTD of RBPJ, which is consistent with previous binding studies[27]. Starting at the
132 N-terminus of its RBPID, SHARP forms a β-hairpin motif that binds between the two β–sheets
133 that compose the Ig domain of the CTD. The second β-strand of SHARP, residues 2788-2794,
134 pairs with β-strand βg of the CTD, extending this from a three- to five-stranded β-sheet (Figure
135 2C). The binding mode of SHARP is structurally analogous to how the *Drosophila melanogaster*
136 corepressor Hairless interacts with the CTD of Su(H) (*the fly CSL ortholog*)[18], which is
137 discussed further below. The SHARP/CTD interaction is followed by a short, approximately six
138 residues, linker region that is poorly ordered and makes no contacts with RBPJ. The C-terminal
139 portion of the SHARP RBPID binds in an extended fashion across the BTD in a manner that is
140 structurally similar to the RAM domain of NICD[15,29,30], and the corepressors FHL1 and RITA1
141 (Figure 2A-B and described below)[13,19]. The complex between SHARP and RBPJ is largely
142 driven by hydrophobic interactions between nonpolar side chains on SHARP, and the CTD and
143 BTD of RBPJ (Figure 2B); with SHARP residue L2791, as well as V2789 and Y2793, anchoring
144 its interaction with the CTD; and I2811 anchoring the interaction between SHARP and the BTD.
145 Additionally, there are key ionic interactions that appear to play auxiliary roles in complex
146 formation, including salt bridges between E2786 of SHARP and R438 of the CTD (Figure 2C),
147 and K2807 of SHARP and the BTD residue E259 (Figure 2B). It should also be mentioned that
148 when complexed with SHARP, RBPJ maintains similar nonspecific and specific contacts with
149 DNA, suggesting that SHARP binding does not affect the affinity of RBPJ for DNA, which is also
150 consistent with previous binding studies[27].

151 As shown in Figure 2C, SHARP binding to RBPJ induces a structural change in CTD
152 that results in translation of β-strands βf and βg outward, modestly expanding the CTD by as
153 much as ~4 Å. A significant structural rearrangement is also observed for the loop that connects
154 strands βe with βf, which strikingly repositions W441 from a buried to a solvent exposed

155 conformation when comparing unbound RBPJ with the RBPJ/SHARP complex (Figure 2C). The
156 repositioning of W441 allows for E2786 of SHARP to form a salt bridge with R438 of RBPJ. This
157 structural rearrangement has not been observed for any other CSL structure determined to
158 date.
159

160 **Structural comparison of coregulator binding sites on RBPJ**

161 The intracellular domain of Notch (NICD) together with Mastermind (MAM) and RBPJ form a
162 transcriptionally active ternary complex[6]. NICD interacts with high affinity to RBPJ[30-33], binding
163 the BTD and CTD of RBPJ via its RAM and ANK domains, respectively[15,16]. Figure 3A
164 compares the interfaces that SHARP and NICD/MAM use to interact with RBPJ, illustrating the
165 overlap of these binding sites. There is partial overlap of the SHARP and ANK/MAM binding
166 sites on the CTD of RBPJ, whereas there is completely overlapping binding of SHARP and the
167 RAM domain of NICD on the BTD of RBPJ. While SHARP and ANK/MAM use different
168 strategies and target different key residues to interact with the CTD, clearly binding of SHARP
169 and ANK/MAM to the CTD is mutually exclusive (Figure 3A). Despite the absence of sequence
170 similarity between SHARP and the RAM domain of NICD, unexpectedly, SHARP interacts with
171 the BTD in a manner that is structurally virtually identical to how RAM, as well as the
172 corepressors FHL1 and RITA1, interacts with BTD (Figure 3B). As shown in Figure 3B, RAM
173 and other coregulators that bind BTD have a characteristic hydrophobic tetrapeptide sequence
174 (-ϕWϕP-) that is essential for binding BTD and serves as the linchpin for high affinity
175 interactions. SHARP is lacking this and other conserved elements that contribute to interactions
176 with BTD[31]. However, a structural alignment of SHARP with RAM and other BTD-binders
177 reveals some sequence conservation of hydrophobic residues that play important roles in
178 SHARP-RBPJ complex formation, including I2804, A2806, I2808, I2811, and P2812 (Figure
179 3B).

180 The corepressor Hairless is the major antagonist of Notch signaling in *Drosophila* and
181 directly binds the CTD of Su(H) (fly *CSL* ortholog) with high affinity in order to repress Notch
182 target gene transcription in flies[18,34,35]. While there is no sequence similarity between SHARP
183 and Hairless, these two corepressors have evolved to bind the same CTD interface on RBPJ
184 and Su(H) (Figure 3C). However, there are major structural differences in how SHARP and
185 Hairless form complexes with the CTD. In contrast to SHARP, which only induces a modest
186 conformational change in CTD, Hairless binding dramatically opens up the Ig domain of CTD,
187 interacting with residues that form the hydrophobic core of CTD[18]. This allows Hairless to bind
188 exclusively to the CTD with high affinity[34].

189 The CTD is structurally similar to the RHR-C domains of transcription factors, such as
190 NF-κB and NFAT[17]. Figure 4A shows the overlay of the CTD from RBPJ with the RHR-C
191 domain from NFAT. Importantly, the CTD deviates from canonical RHR-C domains by the
192 absence of β-strand a′ (βa′), which lies between the two β–sheets that compose the Ig domain
193 of a canonical RHR-C domain. Strikingly, SHARP binding to the CTD serves as a structural
194 surrogate for βa′, occupying this region in the complex structure (Figure 4A), which has
195 interesting implications for how binding sites have evolved on RBPJ and will be discussed
196 further below (Figure 4B).

197

198 **Binding analysis of RBPJ and SHARP mutants**

199 To gain further insights into RBPJ/SHARP complex formation, SHARP function, and to validate
200 our structural studies, we used a combination of assays, both *in vitro* and in cells, to analyze
201 structure-based mutants of RBPJ and SHARP. As shown in Figure 5 and Tables 2 and 3, we
202 used isothermal titration calorimetry (ITC) to quantitate binding between SHARP and RBPJ
203 mutants. SHARP binds RBPJ with high affinity (K_d~5nM, Figure 5A and Table 2), wherein

204 binding is enthalpically driven and entropically unfavorable, in accordance with the RBPID of
205 SHARP being an intrinsically disordered region[27]. Consistent with its side chain burying ~84 Å^2
206 in the SHARP-CTD complex, mutation of L2791 to alanine (L2791A) in SHARP resulted in
207 greater than 350 fold decrease in binding (ΔΔG°=3.4kcal/mol, Figure 5C and Table 2). The
208 SHARP mutants V2789A and Y2793A (Figure 5B,D and Table 2) also significantly reduced
209 binding to RBPJ by >10 fold and >20 fold, respectively, in agreement with these residues also
210 burying considerable amounts of surface area at the SHARP-CTD interface (V2789=54 Å^2 and
211 Y2793=118 Å^2). The side chain of SHARP residue I2811 is buried at the BTD-SHARP interface,
212 lying within a small hydrophobic pocket and burying a substantial 160 Å^2. Mutation of I2811 to
213 alanine (I2811A) results in more than a 60 fold reduction in binding (Figure 5F and Table 2).
214 Mutation of K2807, which makes electrostatic interactions with E259 of the BTD, to alanine
215 results in a much more modest effect on binding (~6 fold, Figure 5E and Table 2). Consistent
216 with SHARP binding independently to the BTD and CTD, which results in an avidity effect[27],
217 single alanine mutants are unable to completely abrogate binding. However, the SHARP double
218 mutant L2791A/I2811A, which targets mutations to key residues that interact with the BTD and
219 CTD, results in a complete loss of binding in our ITC studies (Table 2).

220 Similarly, we performed ITC binding studies with structure-based RBPJ mutants and
221 native SHARP. We performed differential scanning fluorimetry (DSF) to confirm that our RBPJ
222 mutants are correctly folded (Figure S2A); EMSA to show that our RBPJ mutants bind DNA
223 similarly to wild-type (WT) (Figure S2B); immunofluorescence microscopy to demonstrate that
224 our RBPJ mutants properly localize to the nucleus (Figure S2C); and coimmunoprecipitation
225 (CoIP) from cells to show that our RBPJ mutants still bind NICD (Figure S2D). However, we
226 were unable to purify and test by ITC some RBPJ mutants that target key residues in CTD-
227 SHARP complex, *e.g.* F468A, as these residues are buried within the hydrophobic core of the
228 CTD and are required for proper folding of RBPJ. Nonetheless, as shown in Figure 5I and Table
229 3, the mutation of L388, which buries ~103 Å^2 in the complex, to alanine results in an

230 approximately 70 fold reduction in binding. Whereas the CTD mutants L386A, L397A, and
231 L466A had only a minor effect on SHARP binding (Table 3), consistent with these residues
232 burying much less surface area at the CTD-SHARP interface (L386=39 $Å^2$, L397=3 $Å^2$, and
233 L466=44 $Å^2$). Because SHARP binds the BTD of RBPJ in a structurally similar manner to the
234 RAM domain of NICD, and the corepressors FHL1 and RITA1, we used a set of alanine mutants
235 (F261A, V263A, A284V, and Q333A) that we have previously characterized for RAM, FHL1,
236 L3MBTL3, and RITA1 binding to RBPJ (Figure 5G-H and Table 3)[12,13,19,36]. The BTD mutants
237 F261A and A284V, which are more centrally located in the SHARP-BTD interface, have a
238 stronger effect, significantly reducing binding by ~45 fold and ~50 fold, respectively (Figure 5G-
239 H and Table 3). V263A and Q333A, which significantly reduced RAM binding to RBPJ[36], but
240 target more peripheral interactions in the BTD-SHARP complex, only modestly affect binding
241 (Table 3). Interestingly, similar binding trends were observed when these BTD mutants were
242 previously tested for interactions with FHL1 and RITA1[13,19].

243 We also tested our SHARP mutants, and a subset of our RBPJ mutants, in cells using
244 CoIP of exogenously expressed RBPJ and SHARP RBPID proteins, and a mammalian two-
245 hybrid assay (Figure 6). Overall, we observed excellent correspondence between our ITC
246 binding studies and our cellular assays. As shown in Figure 6A, the CoIP of SHARP mutants
247 L2791A and I2811A with RBPJ is greatly reduced compared to wild-type SHARP, and the CoIP
248 of the double mutant L2791A/I2811A is scarcely detectable on the Western blot (Figure 6A, lane
249 9); whereas, the CoIP of SHARP mutants V2789A, Y2793A, K2807A with RBPJ is only
250 modestly affected (Figure 6A, lane 4-6), consistent with our ITC binding studies and the RBPJ-
251 SHARP structure. Similarly, the CoIP of the BTD mutant F261A and the CTD mutant L388A with
252 the RBPID of SHARP are greatly reduced compared to wild-type (Figure 6B, lanes 4-5), but the
253 double mutant F261A/L388A was unable to CoIP SHARP (Figure 6B, lane 6). In our mammalian
254 two-hybrid assays (Figure 6C-E), in which RBPJ and SHARP are fused to VP16 and Gal4,
255 respectively, SHARP mutants L2791A and I2811A have the strongest effect on reporter

256 expression, whereas V2798A, Y2793A, and K2807A only modestly affect reporter expression
257 (Figure 6C). As expected from the complex structure, the SHARP double mutant L279A/I2811A,
258 which does not bind RBPJ in our ITC assays, displayed no more than 1% expression from the
259 reporter compared to wild-type (Figure 6C). The RBPJ mutants F261A and L388A were
260 severely compromised for reporter activity (~1%), whereas no reporter activity was observed for
261 the F261A/L388A double mutant. As a control, all RBPJ mutants fused to the VP16
262 transactivation domain activated a luciferase reporter containing 12 CSL binding sites (Figure
263 6E) and bound DNA in an EMSA (Figure S2B) similar to wild-type.
264

265 **RBPJ/SHARP interaction is required to repress Notch target genes**

266 In order to investigate the contribution of the RBPJ/SHARP interaction in the regulation of Notch
267 target genes in cells, we analyzed the Notch target genes *Hes1* and *Hey1* in a mature T-cell line
268 (MT) that lacks Notch activity. First, to interfere with RBPJ/SHARP-mediated repression in MT
269 cells, we expressed the RBPID of SHARP as a GFP fusion protein either as wild-type (GFP-
270 SHARP/RBPID^{WT}) or the RBPJ-interacting defective L2791A/I2811A mutant (GFP-
271 SHARP/RBPID$^{LI/AA}$) (Figure 7A). Expression of GFP-SHARP/RBPID^{WT} leads to the upregulation,
272 i.e. derepression, of *Hes1* and *Hey1*, whereas GFP-SHARP/RBPID$^{LI/AA}$ has little to no effect on
273 *Hes1 and Hey1* expression (Figure 7A). This suggests that GFP-SHARP/RBPID^{WT}, but not
274 GFP-SHARP/RBPID$^{LI/AA}$, effectively outcompetes endogenous SHARP for binding to RBPJ.
275 Next, we used CRISPR/Cas9 technology to deplete RBPJ (Figure 7B). Consistent with RBPJ
276 repressor function, we observed robust upregulation of *Hes1* and *Hey1* in the absence of RBPJ
277 (Figure 7B). Correspondingly, shRNA-mediated knockdown of RBPJ also resulted in the
278 upregulation of *Hes1* and *Hey1* (Figure 7C). Importantly, reintroduction of wild-type RBPJ
279 (RBPJ^{WT}) in the CRISPR/Cas9-mediated RBPJ depleted background rescues the repression of
280 *Hes1* and *Hey1* Notch target gene expression, whereas the SHARP-interacting defective RBPJ
281 mutant F261A/L388A (RBPJ$^{FL/AA}$) does not (Figure 7D). Altogether, our data demonstrates that

282 the RBPJ/SHARP interaction is strongly required to repress transcription of Notch target genes
283 in cells.
284
285 **Discussion**

286 Notch is a highly conserved signaling pathway that ultimately results in changes in gene
287 expression, a process that is controlled by the transcription factor CSL (Figure 1A)[1,2]. CSL forms
288 an activation complex with the intracellular domain of the Notch receptor (NICD) and the
289 coactivator Mastermind (MAM) to activate transcription from Notch target genes (Figure 1B)[15,16].
290 This activity of CSL is required at all Notch target genes and is conserved in all metazoans. CSL
291 can also function as a transcriptional repressor, by interacting with corepressors such as
292 SHARP[8,9,27], L3MBTL3[12], FHL1[11,19], and RITA1[13,14] in mammals, and Hairless in
293 *Drosophila*[18,34,35]; however, its role as a repressor, in particular in mammals, is not well
294 understood. In order to begin to address this gap in our understanding, here we determine the
295 X-ray structure of the RBPJ-SHARP corepressor complex bound to DNA and use a multitude of
296 *in vitro* and cellular assays to characterize structure based RBPJ and SHARP mutants in order
297 to better understand CSL-corepressor function.

298 Together with previous studies, the complex structure provides a detailed mechanism for
299 how the corepressor SHARP interacts with the transcription factor RBPJ to repress
300 transcription. Prior to binding RBPJ, the RBPID of SHARP is intrinsically disordered[27], which
301 then forms a bipartite interaction with RBPJ. As shown in Figure 2, the N-terminal portion of the
302 RBPID assumes a β-hairpin motif that interacts with the CTD of RBPJ, resulting in a modest
303 conformational change in the CTD; the SHARP-CTD interaction is followed by a poorly
304 structured linker and then an extended region that binds across a nonpolar surface on the BTD.
305 Thus, SHARP forms a high affinity complex with RBPJ by interacting with two distant binding
306 surfaces on RBPJ, which individually are low affinity, but when tethered by the linker region

307 result in an avidity effect[27]. RBPJ-SHARP complex formation localizes the RRM and SPOC
308 domains of SHARP to Notch target genes (Figure 1C). In the case of SPOC, this recruits other
309 factors involved in transcriptional repression, such as NCoR/SMRT[20,24], CtIP (C-terminal binding
310 protein interacting protein)/CtBP (C-terminal binding protein)[23], and ETO (eight-twenty-one)[22],
311 as well as the KMT2D coactivator complex[24]. Whether the RRM domains of SHARP recruit Xist
312 lncRNA or other lncRNAs, such as SRA (steroid receptor coactivator)[37], to Notch target genes
313 remains to be determined

314 Analogous to SHARP, NICD also binds the BTD and CTD of RBPJ (Figure 1B and 3A);
315 however, the two complexes with RBPJ are mutually exclusive (Figure 3A) and the distribution
316 of binding energies for surfaces on RBPJ is distinct. In mammals, the RAM domain of NICD
317 forms a high affinity interaction with the BTD[30-33], comparable to the affinity of SHARP for
318 RBPJ[27], and is structurally very similar to how SHARP interacts with the BTD despite no
319 sequence similarity between the two proteins (Figure 3B). The ANK domain of NICD, however,
320 binds the CTD of RBPJ in a manner that is structurally very different than SHARP and the ANK-
321 CTD interaction is extremely weak, barely discernible in some binding assays[27,30,32,33]. MAM is
322 then required to stabilize the RBPJ-NICD-MAM ternary complex. The functional consequences
323 of these structural and binding differences between SHARP and NICD are currently unclear, but
324 it may be important for the dynamic association/dissociation of RBPJ-coregulator complexes
325 and the lifetimes of these complexes in the nucleus. Certainly, single molecule studies of wild-
326 type and mutant SHARP molecules will be important for addressing the dynamics of RBPJ-
327 coregulator complexes in live mammalian cells.

328 Our cellular studies clearly demonstrate that CRISPR/Cas9-mediated depletion of RBPJ
329 in MT cells results in derepression of the well-established Notch target genes *Hes1 and Hey1*
330 (Figure 7)[38]. Moreover, reconstitution of repression by wild-type RBPJ, but not a SHARP-binding
331 mutant, strongly suggests that SHARP is the primary corepressor that mediates repression via

332 RBPJ at Notch target genes in lymphocytes, and likely other cells and tissues, which is
333 consistent with previous *in vivo* studies of SHARP in mice[8,39,40]. These data are also consistent
334 with research in other experimental systems that show that loss of CSL results in transcriptional
335 derepression at some, but not all, Notch target genes[41,42]. Why RBPJ-SHARP corepressor
336 complexes are recruited to some Notch targets, but not others, remains an open question.
337 Clearly, the use of RBPJ mutants defined here that affect SHARP interactions, but leave NICD
338 interactions largely intact, will be instrumental in addressing this and other questions regarding
339 the function of RBPJ as a transcriptional repressor.

340 Classical models of transcriptional regulation in the Notch pathway posit that CSL is
341 constitutively bound to DNA, and that corepressors are replaced by NICD when signaling is
342 activated[43,44]. Given the comparable high affinities of both SHARP and NICD for RBPJ[27,30], as
343 well as the more modest affinity of CSL for DNA (~0.5-1.0 μM)[45,46], it is difficult to reconcile how
344 cofactor exchange on DNA, *i.e.* NICD replacing SHARP on RBPJ, might work at the molecular
345 level. The affinities rather suggest that preformed RBPJ-corepressor complexes and RBPJ-
346 NICD-MAM coactivator complexes are dynamically associating/dissociating with sites on the
347 DNA. This scenario is supported by recent data by Bray and colleagues investigating the DNA-
348 binding dynamics of Su(H) complexes with NICD and Hairless in Notch-ON and Notch-OFF
349 states in the salivary gland of *Drosophila melanogaster*[47].

350 In contrast to the CSL-NICD-MAM activator complex, CSL-corepressor interactions
351 appear to be less conserved across disparate organisms. For example, while SHARP, also
352 known as SPEN in *Drosophila* and DIN-1 in *C. elegans*, is conserved from nematodes to flies to
353 mammals[48], the RBPID of SHARP is only conserved in vertebrates[27]. Similarly, the corepressor
354 Hairless, which is the major antagonist of Notch signaling in *Drosophila*, is not conserved
355 outside of insects and crustaceans[49]. However, while the corepressors that bind CSL are not
356 strictly conserved across disparate organisms, interestingly, the corepressor binding sites on

357 CSL are conserved. For example, SHARP, as well as the corepressors RITA1, FHL1, and likely
358 L3MBTL3, binds to the BTD of RBPJ in a structurally similar manner (Figure 3B); and strikingly,
359 despite no sequence conservation between SHARP and Hairless, both proteins bind to the
360 same surface of the CTD of CSL (Figure 3C). Thus, it seems likely that other species-specific
361 transcriptional corepressors that bind CSL will be identified, but they will likely utilize the
362 aforementioned conserved binding surfaces on the BTD and CTD to interact with CSL.

363 In a broader context, CSL provides an interesting example for how ligand binding sites
364 evolve in proteins. CSL is composed of two types of domains – the NTD and CTD are
365 immunoglobulin domains that are structurally related to the rel homology region (RHR) of
366 proteins, such as NF-κB and NFAT, and the BTD contains a β-trefoil fold that is structurally
367 related to growth factors such as interleukins and FGF[17]. As shown in Figure 4A, the canonical
368 RHR-C fold contains a β-strand, βa', that lies in between β-strands βa and βg; however, the
369 CTD of CSL is missing βa' typically found in RHR-C domains. The ligand, in this case the
370 corepressor SHARP, serves as a structural surrogate binding precisely in the region where the
371 missing βa' strand would lie. Strikingly, this is the second example in CSL proteins where this
372 type of ligand evolution has occurred. The first example, as shown in Figure 4B, was uncovered
373 following the structure determination of the CSL-NICD-MAM activation complex[15], whereby it
374 was shown that the BTD of CSL is atypical, as it deviates from the canonical β-trefoil fold such
375 that it is missing two of the 12 strands of the consensus fold[17]. In this instance, the ligand, the
376 RAM domain of NICD, again serves as a structural surrogate, binding across the BTD exactly
377 where the two missing β-strands would normally lie.

378 Finally, because of its association with human disease, there have been wide-ranging
379 efforts to pharmacologically target the Notch pathway, but the majority of this work has focused
380 on reagents that blunt overactive Notch signaling, *e.g.* in T-cell acute lymphoblastic leukemia[4,5].

381 However, there are numerous human diseases, including certain types of cancer,
382 cardiovascular defects, and congenital syndromes that are associated with insufficient Notch
383 signaling[3]. Our structure-function studies of the RBPJ-SHARP corepressor complex provide a
384 roadmap for developing reagents that lead to the derepression of Notch target genes, which
385 have the potential to become new treatment options for diseases connected to deficiencies in
386 Notch signaling.

387

388 **Methods**

389 ***Protein expression and purification***

390 The cloning, expression, and purification of *Mus musculus* core RBPJ, residues 53–474, and
391 SMT3-SHARP, residues 2776-2833, which corresponds to the RBPJ-interacting region, were
392 described previously[27]. An MBP-SHARP fusion protein was used to crystallize the
393 RBPJ/SHARP/DNA complex. SHARP, corresponding to residues 2776-2820, was cloned into
394 pMALX-E, which encodes maltose binding protein with the following surface entropy reduction
395 mutations D82A, K83A, E172A, N173A, and K239A to aide in crystallization. The MBP-SHARP
396 fusion construct was overexpressed in Tuner *E. coli* and cells were lysed by sonication. The
397 lysate was incubated with amylose resin and eluted with 10 mM maltose. The MBP-SHARP
398 fusion protein was further purified by size exclusion chromatography.

399

400 ***Crystallization and Data Collection***

401 RBPJ/MBP-SHARP/DNA complexes were setup in a 1:1.1:1.1 molar ratio and screened for
402 crystallization conditions using an Art Robbins Phoenix Crystallization Robot at 4°C. The
403 RBPJ/MBP-SHARP/DNA complex crystallized in 100mM Bis-Tris pH 6.6, 100mM NaCl, 40%

404 PEG 400, and 200mM NDSB-256. Crystals were harvested, flash frozen in liquid nitrogen,
405 diffraction data were collected at the Advanced Photon Source, beamline 21-ID-F (LS-CAT).
406 The RBPJ/MBP-SHARP/DNA crystals nominally diffract to 2.8Å and belong to the spacegroup
407 $P2_1$ with unit cell dimensions a=54.5 Å, b=231.6 Å, c=90.3 Å, and β=99.88°.

408

409 ***Structure Determination, Model Building, and Refinement***

410 Molecular replacement with Phaser[50] was used to determine the RBPJ/MBP-SHARP/DNA
411 complex structure using the following search models DNA (3BRG), CSL (3IAG), and MBP
412 (3OB4). Two RBPJ/MBP-SHARP/DNA complexes were identified in the asymmetric unit. Phenix
413 was used for the initial stages of refinement[51]. Manual model building was performed with
414 COOT[52]. TLS parameters were generated and the model was subsequently refined using
415 BUSTER[53] and validated with MolProbity[54]. The final RBPJ/MBP-SHARP/DNA model was
416 refined to an R_{work} = 18% and R_{free} = 23% with good overall geometry (see Table 1). PyMOL
417 (The PyMOL Molecular Graphics System, Version 2.0 Schrödinger, LLC) was used to generate
418 figures and perform structural overlays. The PISA server was used to analyze protein
419 interfaces[55].

420 Coordinates and structure factors have been deposited into the Protein Data Bank (XYZ1)

421

422 ***Isothermal titration calorimetry (ITC)***

423 ITC experiments were performed using a Microcal VP-ITC micocalorimeter. For all binding
424 reactions, SMT3-SHARP (2776-2883) at ~100μM was placed in the syringe concentrations and
425 RBPJ (53-474) at ~10 μM was placed in the cell. Titrations consisted of an initial 1μl injection
426 followed by 39 7μl injections. ITC binding experiments were performed in 50 mM sodium

427 phosphate pH 6.5, 150 mM NaCl at 25°C. Samples were buffer matched using size-exclusion
428 chromatography or dialysis. The raw data were analyzed using ORIGIN and fit to a one site
429 binding model.

430

431 ***Cell culture and preparation of cell extracts***

432 Mouse hybridoma mature T (MT) cell line was grown in Iscove's Modified Dulbecco Medium
433 (IMDM, Gibco) supplemented with 2% FCS, 0.3 mg/l peptone, 5 mg/l insulin, nonessential
434 aminoacids and penicillin/streptomycin. Cells were grown at 37°C with 5% CO_2. HeLa (ATCC:
435 CCL2), HEK-293 (ATCC: CRL1573), 293T and *Phoenix*™ packaging cells (*Orbigen*, Inc., San
436 Diego, CA, USA) were cultivated in Dulbecco's Modified Eagle Medium (DMEM, Gibco)
437 supplemented with 10% fetal calf serum (FCS) and penicillin/streptomycin.

438

439 ***DNA transfection***

440 HEK-293 and HeLa cells were transfected using the Nanofectin transfection reagent (PAA)
441 according to the manufacturer's instructions.

442

443 ***Coimmunoprecipitation experiments***

444 HEK-293 cells were transfected with the indicated constructs for expression of GFP- and Flag-
445 tagged wild-type and mutant proteins. 24 hours after transfection cells were lysed with 600 µl
446 CHAPS lysis buffer [10 mM 3-[(3-Cholamidopropyl)dimethylammonio]-1-propanesulfonate
447 hydrate (CHAPS, Merck), 50 mM Tris-HCl (pH 7.8), 150 mM NaCl, 5 mM NaF, 1 mM
448 Dithiothreitol (DTT, Merck), 0.5 mM Phenylmethanesulfonyl fluoride (PMSF, Merck) and 40 µl/ml

449 “Complete Mix” protease inhibitor cocktail (Roche)]. The extracts were incubated with 40 µl
450 agarose-conjugated anti-Flag antibody (M2, Sigma) at 4°C overnight. Precipitates were washed
451 6 to 8 times with CHAPS lysis buffer and finally resuspended in SDS-polyacrylamide gel loading
452 buffer. For Western blotting the proteins were resolved in SDS-polyacrylamide gels and
453 transferred electrophoretically at room temperature to PVDF membranes (Millipore) for 1 h at 50
454 mA using a Tris-glycine buffer system. The membranes were pre-blocked for 1 h in a solution of
455 3% milk powder in PBS-T (0.1% Tween 20 in PBS) before adding antibodies. The following
456 antibodies were used: anti-GFP (7.1/13.1, mouse monoclonal IgG, secondary antibody
457 peroxidase conjugated sheep anti-mouse IgG, NA931V, GE healthcare) or anti-Flag (M5,
458 Sigma; secondary antibody, NA931V, GE healthcare).

459

460 ***In vitro protein translation***

461 The *in vitro* protein translations were performed using the TNT-assay (#L4610) from Promega
462 according to manufacturer´s instructions. Prior to EMSAs the *in vitro* translations of RBPJ (wt)
463 and mutant proteins were monitored by western blotting using an anti-Flag antibody (M5,
464 Sigma).

465

466 ***Electro Mobility Shift Assay (EMSA)***

467 Reticulocyte lysates from *in vitro* translations were used for electromobility shift assays (EMSAs)
468 in a binding buffer consisting of 10 mM Tris-HCl (pH 7.5), 100 mM NaCl, 0.1 mM EDTA, 0.5 mM
469 DTT, and 4% glycerol. For binding reaction, 2 µg poly(dI-dC) (GE healthcare) and approximately
470 0.5 ng of ^{32}P-labelled oligonucleotides were added. The sequence of the double-stranded
471 oligonucleotide FO-233 (Supplementary Table S1) corresponds to the two RBP-J-binding sites

472 within the EBV TP-1 promoter. Super shifting of complexes was achieved by adding 1 µg of
473 anti-Flag (M5, Sigma) antibody. The reaction products were separated using 5% polyacrylamide
474 gels with 1x Tris-glycine-EDTA at room temperature. Gels were dried and exposed to X-ray
475 films (Kodak).

476

477 ***Fluorescence microscopy***

478 HeLa cells were cultured on glass cover slips in a 25-well plate (Bibby Sterilin Ltd) at a density
479 of 10^5 cells per cm^2. After 16 h cells were transfected with 400 ng of expression plasmids using
480 the Nanofectin transfection reagent (see above). 24 h after transfection cells were rinsed with
481 PBS, fixed with 4% paraformaldehyde (PFA, Merck) in PBS (pH = 7.5). Specimens were
482 embedded in "ProLong© Gold antifade" reagent (Invitrogen) supplemented with 2-(4-
483 carbamimidoylphenyl)-1H-indol-6-carboximidamide (DAPI) and stored at 4 °C overnight.
484 Pictures were taken using a fluorescence microscope (IX71, Olympus) equipped with a digital
485 camera (C4742, Hamamatsu), and a 100-W mercury lamp (HBO 103W/2, Osram). The
486 following filter sets were used: Green, (EGFP) ex: HQ470/40, em: HQ525/50, blue (DAPI)
487 D360/50, em: D460/50.

488

489 ***Luciferase assay***

490 HeLa cells were seeded in 48-well plates at a density of 20 x 10^4 cells. Transfection was
491 performed with Nanofectin reagent (see above) using 1 µg of reporter plasmid alone or together
492 with various amounts of expression plasmid (given in the corresponding figure legends). After
493 24 h luciferase activity was determined from at least six independent experiments with 20 µl of

494 cleared lysate in an LB 9501 luminometer (Berthold) by using the luciferase assay system from
495 Promega.

496

497 ***Infection of hybridoma mature T-cell line***

498 5 x 10^6 *Phoenix*™ cells were seeded and 24 h later they were transfected with the plasmid DNA
499 of choice. Briefly, 20 μg of DNA were mixed with 860 μl of H_2O and 120 μl of 2 M $CaCl_2$ and
500 mixed by vortexing. The DNA solution was transferred dropwise to 1 ml of 2 x HBS buffer (50
501 mM HEPES pH 7.05, 10 mM KCl, 12 mM Glucose, 280 mM NaCl, 1.5 mM $NaHPO_4$) while
502 vortexing and the solution was incubated 20 min at room temperature. In the meantime, 25 μM
503 Chloroquine solution (Sigma-Aldrich) was added to the *Phoenix*™ cells (1 μl/ml) and the cells
504 were incubated for 10 min. The DNA solution was added to the cells and 12 h later the medium
505 was replaced. After 24 h of incubation, the medium containing the retroviral suspension was
506 filtered and 2 mg/ml Polybrene (Sigma-Aldrich) solution was added (1 μl/ml). Fresh medium was
507 added to the *Phoenix*™ cells that were maintained in culture for further infections. The retroviral
508 solution was used for spin infection of MT cells by centrifuging 45 min at 1800 rpm at 37°C. In
509 total, four spin infections were performed over two days. Positively infected cells were selected
510 with puromycine (Serva) or blasticidin (Gibco) and, eventually, GFP positivity was analyzed
511 using a BD FACS Calibur.

512

513 ***Generation of CRISPR/Cas9* depleted MT cells**

514 CRISPR/Cas9 *Rbpj* depleted MT cells were generated as follows: 3 x 10^6 293T cells were
515 seeded and, after 24 h, transfected with 2.5 μg psPAX, 1 μg pMD2G and 3.33 μg of the desired
516 lentiCRISPR v2 vector using Lipofectamine 2000 Transfection Reagent (Invitrogen 11668-019)

517 accordingly to manifacturer's instructions. After at least 6 h of incubation at 37°C the medium
518 was replaced with fresh one and 48 h post-transfection the supernatant was filtered,
519 supplemented with polybrene and used for infection of MT cells. Positively infected cells were
520 selected with puromycin and dilutions were performed to establish single cell clones. Individual
521 clones were screened by Western blotting versus RBPJ.
522

523 ***shRNA knockdown***

524 For the knockdown in MT cells, the pLKO.1 TRC1 shRNA library (SIGMA-ALDRICH) was used.
525 Transfection of 293T cells and infection and selection of MT cells was performed as previously
526 described. Sequence of the hairpins used in this study is indicated in Table S1.

527

528 ***Constructs***

529 The expression plasmid pcDNA3-Flag-mNotch-1-IC (Flag-NICD) and the luciferase reporter
530 construct pGa981/6 (12 x CSL-RE-LUC) were previously described[14]. The Gal4-reporter
531 plasmid pFR-Luc (5 x Gal4-RE-LUC) was previously described[9]. The pMSCV-FLAG-hRBP-J
532 IRES Blasticidin was kindly provided by Dr. R. Liefke. All oligonucleotides used in this study are
533 listed in Table S1. PCR products were cloned in the pSC-A-amp/kan (Agilent Technologies
534 240205-5), digested with the selected restriction enzymes (New England Biolabs) and cloned
535 into the destination vectors accordingly to Table S2. All plasmids were analyzed by sequencing.
536 The pcDNA 3.1 Flag2 (Invitrogen) was commercially acquired while the pMY BioTip60 IRES-
537 GFP was previously described.

538 An engineered CRISPR/Cas9 resistant mouse RBPJ cDNA was synthetized at
539 GENEART/Life Technologies and inserted into the pcDNA3.1 Flag2 via NotI digestion. The

540 RBPJ mutants R218H, F261A, L388A and the F261A/L388A double mutant was generated by
541 site directed mutagenesis using the QuikChange II XL Site-Directed Mutagenesis Kit (Agilent
542 Technologies 200521-5) accordingly to manufacturer's instructions with primers listed in Table
543 S1 and using the pcDNA3.1 Flag-mRBPJ wt CRISPR/Cas9 resistant plasmid as template. The
544 mRBPJ wt and RBPJ F261A/L388A CRISPR/Cas9 resistant cDNAs were subcloned into the
545 pMY-Bio-IRES Blasticidin. The mouse RBPJ-VP16 expression plasmids (pcDNA3.1-Flag-2-
546 mRBPJ-VP16 wt, F261A, L388A and F261A/L388A) were constructed as follows: The stop
547 codon was deleted by a mRBP-J specific PCR fragment (mRBP_VP16_UP, mRBP-TAA_DO)
548 resulting in the pcDNA3.1-Flag-2-mRBPJΔstop constructs. A VP16 specific PCR-fragment
549 (VP16_XhoI_UP, VP16_XbaI_DO) was inserted into the corresponding sites of pcDNA3.1Flag-
550 2-mRBPJΔstop constructs resulting in the pcDNA3.1-Flag2-mRBPJ-VP16 plasmids. The Gal-4-
551 Mint (2776-2833) and the EGFP-Mint (2776-2833) constructs were generated by PCR assisted
552 cloning (Gal-Mint_F, Gal-Mint_R) into the BamHI/XbaI sites of pFa-CMV (Stratagene) and
553 pEGFP-C1 (Clontech), respectively. The mutated constructs (V2785A, Y2793A, K2807A,
554 I2811A, L2791A and I2811A/L2791A) were obtained by site directed mutagenesis.

555 The lentiCRISPR v2 was a gift from Dr. F. Zhang (Addgene plasmid # 52961). The
556 CRISPR/Cas9 guides were designed using the online tool available at http://crispr.mit.edu/. The
557 desired 5' overhangs were added and oligos were phosphorylated, annealed and ligated into
558 the lentiCRISPRv2 predigested with BsmBI.

559

560 ***RNA extraction, RT-PCR and qPCR***

561 Total RNA was purified using Trizol reagent (Ambion, 15596018) accordingly to manufacturer's
562 instructions. 1 μg of RNA was reverse transcribed in cDNA using random hexamers and M-
563 MuLV reverse transcriptase (NEB). qPCRs were assembled with Absolute QPCR ROX Mix

564 (Thermo Scientific, AB-1139), gene-specific oligonucleotides and double-dye probes (see Table
565 S1) and analyzed using the StepOne Plus Real Time PCR system (Applied Biosystem). Data
566 were normalized to the housekeeping gene *glucuronidase* β (*GusB*).

567 ***Preparation of protein extracts and Western Blotting from MT cells***

568 Whole Cell Extract (WCE) was prepared as follows. Briefly, cells were washed twice in PBS,
569 lysed in WCE buffer (20 mM Tris-HCl pH 8.0, 150 mM NaCl, 1% NP-40, 10% glycerol, 0.5 mM
570 Na_3VO_4, 10 mM NaF, 1 mM PMSF, 1 x Protease inhibitor cocktail mix) and incubated 20 min on
571 ice. After centrifuging 15 min at 13200 rpm at 4°C, the supernatant was recovered.

572 The Nuclear Extract (NE) from MT cells overexpressing the SHARP constructs was
573 prepared as follows. Briefly, cells were washed with PBS and resuspended in Buffer A (20 mM
574 Hepes pH 7.9 / 20 mM NaCl / 5 mM $MgCl_2$ / 10% glycerol / 0.2 mM PMSF) at the concentration
575 of 1 x 10^6 cells/ml. The cell suspension was incubated 20 min on ice and mixed by vortexing.
576 After 5 min centrifugation at 4000 rpm at 4°C, the pellet was washed twice in PBS and
577 resuspended in Buffer C (20 mM Hepes pH 7.9 / 300 mM NaCl / 0.2% NP-40 / 25% glycerol / 1
578 mM $MgCl_2$/ 0.2 mM PMSF / 1 x Protease inhibitor mix / 0.3 mM DTT) at the concentration of 1 x
579 10^6 nuclei/100 μl. After 20 min of incubation on ice, the nuclei suspension was centrifuged 5 min
580 at 13200 rpm at 4°C and the supernatant was collected.

581 The NE from MT cells overexpressing the RBPJ constructs was prepared as follows.
582 Briefly, 10 x 10^6 cells were washed with PBS and resuspended in 200 μl of Buffer 1 (10 mM
583 Hepes pH 7.9 / 10 mM KCl / 0.1 mM EDTA / 0.1 mM EGTA / 1 mM ßME, supplemented with
584 PMSF). The cell suspension was incubated 10 min on ice, 5 μl of 10% NP-40 were added and
585 mixed by vortexing. After 10 sec of centrifugation at 13000 rpm at 4°C, the nuclei pellet was
586 washed twice in 500 μl of Buffer 1 and resuspended in 100 μl of Buffer 2 (20 mM Hepes pH 7.9
587 / 400 mM NaCl / 1 mM EDTA / 1 mM EGTA / 1 mM ßME, supplemented with PMSF). After 20

588 min of incubation on ice, the nuclei suspension was centrifuged 10 min at 13000 rpm at 4°C and
589 the supernatant was collected for further analysis.

590 Protein concentration was measured by Bradford assay (Sigma-Aldrich) and samples
591 were boiled after adding SDS-polyacrylamide gel loading buffer. Samples were resolved by
592 SDS-Page and analyzed by Western blotting using antibodies against GAPDH (abcam,
593 ab8245), GFP (Roche, 11814460001) or TBP (Santa Cruz, sc-273). Briefly, membranes were
594 blocked in 5% milk, 1x TBS, 0.1% Tween-20 (TBS-T) and primary antibodies were diluted in 5%
595 milk, TBS-T. After incubation over night at 4°C, membranes were washed in TBS-T, secondary
596 antibodies against mouse (Cell Signaling, #7076S) or rabbit (Cell Signaling, #7074S) were
597 diluted in 5% milk TBS-T and finally membranes were washed in TBS-T.

598 In the case of the RBPJ Western blotting the procedure was as follows. Briefly,
599 membranes were blocked in 5% milk, 1x TBS and the RBPJ antibody (Cosmo Bio Co. LTD,
600 2ZRBP2) was diluted 1:1000 in 5% BSA, 1x TBS, 0.3% NP40. After incubation over night at
601 4°C, membranes were washed three times 15 min each in 1x TBS / 0.5 M NaCl / 0.5% Triton X-
602 100 and the secondary antibody against rat (Jackson ImmunoResearch, 112-035-072) was
603 diluted 1:5000 in 5% BSA, 1x TBS, 0.3% NP-40. Membranes were washed three times 15 min
604 each in 1x TBS / 0.5 M NaCl / 0.5% Triton X-100. All membranes were finally incubated with
605 ECL solution and chemiluminescence was detected with a light sensitive film.

606

607 **Acknowledgements**

608 We thank Roswitha Rittelmann, Sabine Schirmer, and Thomas Schmidt-Wöll for excellent
609 technical assistance. This work was supported by National Institutes of Health Grants
610 5R01CA178974 (RAK). It was also supported by the collaborative research grant TRR81 and
611 the grant (BO 1639/9-1) by the DFG (German Research Foundation) and the Excellence Cluster

612 for Cardio Pulmonary System (ECCPS) in Giessen to TB and the University Medical Center
613 Giessen and Marburg (UKGM to BG). This work was further supported by German Research
614 Foundation (DFG) Grant SFB1074/A3 and by the BMBF (Federal Ministry of Education and
615 Research, research nucleus SyStAR) to FO. LP is supported by the DFG (GRK 2253 – HEIST).
616 This research used resources of the Advanced Photon Source, a U.S. Department of Energy
617 (DOE) Office of Science User Facility operated for the DOE Office of Science by Argonne
618 National Laboratory under Contract No. DE-AC02-06CH11357.

619
620
621
622
623
624
625
626
627
628
629
630
631
632
633
634
635
636
637

638 **Table 1: X-ray Data collection and refinement statistics.**

Data Collection Statistics

Resolution (Å)	50.0 – 2.8 (2.85 – 2.78)
Space Group	$P2_1$
Wavelength (Å)	0.97872
Unit Cell a, b, c (Å)	54.5, 231.6, 90.3
Unit Cell α, β, γ (°)	90.00, 99.9, 90.00
R_{merge}	0.084 (0.48)
$I/\sigma I$	14.9 (2.3)
Completeness (%)	99.3 (97.6)
Redundancy	3.7 (3.4)

Refinement Statistics

R_{work}/R_{free} (%)	19.4 / 22.8
Number of reflections	54,503
Number of atoms	13,392
Complexes/asymmetric unit	2
Wilson B/Mean B value ($Å^2$)	72.68 / 77.80
RMSD Bond Lengths (Å)	0.008
RMSD Bond Angles (°)	0.96
Ramachandran (favored/outliers)	96.34% / 0.37%

639 Highest resolution shell shown in parentheses.

640
641
642
643
644
645
646
647
648
649
650
651
652

653 **Table 2: Calorimetric binding data for SHARP mutants and native RBPJ**

SHARP	K (M^{-1})	K_d (uM)	$\Delta G°$ (kcal/mol)	$\Delta H°$ (kcal/mol)	$-T\Delta S°$ (kcal/mol)	$\Delta\Delta G°$ (kcal/mol)
WT	$2.0 \pm 0.5 \times 10^8$	0.005	-11.3 ± 0.1	-13.5 ± 0.4	2.2 ± 0.3	--
V2789A	$1.9 \pm 1.3 \times 10^7$	0.067	-9.9 ± 0.4	-11.0 ± 0.9	1.1 ± 1.2	1.4
L2791A	$5.8 \pm 1.0 \times 10^5$	1.75	-7.9 ± 0.1	-7.8 ± 0.8	-0.1 ± 0.7	3.4
Y2793A	$8.7 \pm 2.5 \times 10^6$	0.122	-9.4 ± 0.2	-9.0 ± 0.2	-0.4 ± 0.4	1.9
K2807A	$3.6 \pm 0.8 \times 10^7$	0.029	-10.3 ± 0.2	-13.3 ± 0.1	3.0 ± 0.1	1.0
I2811A	$3.3 \pm 0.6 \times 10^6$	0.316	-8.9 ± 0.1	-12.3 ± 0.2	3.4 ± 0.2	2.4
L2791A/I2811A	NBD	---	---	---	---	---

654 All experiments were performed at 25°C. NBD represents no binding detected.
655
656
657
658 **Table 3: Calorimetric binding data for native SHARP and RBPJ mutants**

	RBPJ	K (M^{-1})	K_d (uM)	$\Delta G°$ (kcal/mol)	$\Delta H°$ (kcal/mol)	$-T\Delta S°$ (kcal/mol)	$\Delta\Delta G°$ (kcal/mol)
	WT	$2.0 \pm 0.5 \times 10^8$	0.005	-11.3 ± 0.1	-13.5 ± 0.4	2.2 ± 0.3	--
BTD mutants	F261A	$4.5 \pm 0.9 \times 10^6$	0.23	-9.1 ± 0.1	-9.9 ± 0.5	0.8 ± 0.4	2.2
	V263A	$3.2 \pm 0.4 \times 10^8$	0.003	-11.6 ± 0.1	-18.3 ± 0.8	6.7 ± 0.9	-0.3
	A284V	$4.0 \pm 1.0 \times 10^6$	0.27	-9.0 ± 0.2	-12.9 ± 0.6	3.9 ± 0.7	2.3
	Q333A	$2.6 \pm 0.3 \times 10^8$	0.004	-11.4 ± 0.1	-16.8 ± 0.7	5.4 ± 0.7	-0.1
CTD mutants	L386A	$7.5 \pm 3.5 \times 10^7$	0.016	-10.7 ± 0.3	-13.2 ± 0.4	2.5 ± 0.7	0.6
	L388A	$2.6 \pm 0.5 \times 10^6$	0.391	-8.7 ± 0.1	-7.5 ± 0.6	-1.2 ± 0.7	2.6
	L397A	$4.2 \pm 0.8 \times 10^7$	0.025	-10.4 ± 0.1	-11.3 ± 0.2	0.9 ± 0.3	0.9
	L466A	$9.6 \pm 2.4 \times 10^7$	0.011	-10.9 ± 0.1	-13.3 ± 0.2	2.4 ± 0.2	0.4
BTD/CTD	F261A/L388A	NBD	---	---	---	---	---

659 All experiments were performed at 25°C. NBD represents no binding detected.
660
661
662
663
664
665
666
667
668
669
670

671 **Table S1.** Oligonucleotides used for plasmid construction, EMSAs, shRNAs, CRISPR/Cas9,
672 and qPCR experiments.

Constructs		
Blasticidin NotI fw	5'-GCG GCC GCC CCC CCC CCC TAA CGT TA-3'	
Blasticidin SalI rev	5'-GTC GAC TTA GCC CTC CCA CAC ATA ACC AGA GG-3'	
Puro_EcoRI_F	5´-CTA TGA ATT CGG TGT GGA AAG TCC CCA GG-3´	
Puro_HindIII_R	5´-TTC AAA GCT TTC AGG CAC CGG GCT TGC G-3´	
mRBP_VP16_F	5´-GCC AGC CAG TCC AGG TTC C-3´	
mRBP-TAA_R	5´-ATC TCG AGG GAC ACC ACG GTT GCT GTG G-3´	
VP16_XhoI_F	5´-ATC TCG AGA GCT TGG CCC CCC CG-3´	
VP16_XbaI_R	5´-CAT CTA GAT TAC CCA CCG TAC TCG TCA ATT CCA AG-3´	
Gal_Mint_F	5´-ATG GAT CCG GCG CGG GCC TGC G-3´	
Gal_Mint_R	5´-CCT CTA GAC TAG AGC GGC CG-3´	
shRNA		
Rbpj_sh1	5´-GCA GAC TCA TTG GGC TAC ATT-3´	
Rbpj_sh4	5´-CCC TGT GCG TTT ATT GGA ATA-3´	
CRISPR/Cas9 guides		
sgRbpj_oligo_3	5´-GCT TGA CAG TCT GCC CGT AA-3´	
sgRbpj_oligo_4	5´-CGA CGA CGA GTC GGA AGG AG-3´	
Site directed mutagenesis		
mRBPJ_F261A_F	5´-GAA AGT GAG GGG GAA GAG GCC ACA GTT AGA GAT GGC TAC-3´	
mRBPJ_F261A_R	5´-GTA GCC ATC TCT AAC TGT GGC CTC TTC CCC CTC ACT TTC-3´	
mRBPJ_L388A_F	5´-CTG TCG TAG AAA GTC TTC AGG CGA ATG GCG GCG GGG ACG TAG-3´	
mRBPJ_L388A_R	5´-CTA CGT CCC CGC CGC CAT TCG CCT GAA GAC TTT CTA CGA CA-3´	
mRBPJ_R218H_F	5'-CGA AGG TGG CAC TGT TCA ATC ACC TTC GGT CCC AGA CAG-3'	
mRBPJ_R218H_R	5'-CTG TCT GGG ACC GAA GGT GAT TGA ACA GTG CCA CCT TCG-3'	
Mint-I2811A-F	5´-GAT CAG CCA GGC CCC TCC AG-3´	
Mint-I2811A-R	5´-CTG GAG GGG CCT GGC TGA TC-3´	
Mint-V2789A-F	5´- catcagaaggggtcgcgctgctgagctactc -3´	
Mint-V2789A-R	5´- gagtagctcagcagcgcgacccttctgatg -3´	
Mint-Y2793A-F	5´- gtcgtgctgctgagcgcctcgggacagaagac -3´	
Mint-Y2793A-R	5´- gtcttctgtcccgaggcgctcagcagcacgac -3´	
Mint-K2807A-F	5´- agggatctggctgatcgcagcactgatccgctgg -3´	
Mint-K2807A-R	5´- ccagcggatcagtgctgcgatcagccagatccct -3´	
Mint-L2791A-F	5´- gtcccgagtagctcgccagcacgacccctt -3´	
Mint-L2791A-R	5´- aaggggtcgtgctggcgagctactcgggac -3´	

Mint-I2811A-F	5´- gcgctggctggaggggcctggctgatcttagc -3´	
Mint-I2811A-R	5´- gctaagatcagccaggcccctccagccagcgc -3´	
real time PCR		
	Mus musculus	*Probe*
GusB_F	5´-TGT GGG CAT TGT GCT ACC T-3´	25
GusB_R	5´-ATT TTT GTC CCG GCG AAC-3´	
Hes1_F	5´-ACA CCG GAC AAA CCA AAG AC-3´	99
Hes1_R	5´-CGC CTC TTC TCC ATG ATA GG-3´	
Hes1_2_F	5´-TGC CAG CTG ATA TAA TGG AGA A-3´	20
Hes1_2_R	5´-CCA TGA TAG GCT TTG ATG ACT TT-3´	
Tbp_F	5´-GGG GAG CTG TGA TGT GAA GT-3´	97
Tbp_R	5´-CCA GGA AAT AAT TCT GGC TCA T-3´	
Hey1_F	5´-CAT GAA GAG AGC TCA CCC AGA-3´	17
Hey1_R	5´-CGC CGA ACT CAA GTT TCC-3´	
EMSA		
FO233_F	5´-CCT GGA ACT ATT TTC CCA CGG TGC CCT TCC GCC CA TTT TCC CAC GAG TCG-3´ (RBP-J binding sites underlinded)	
FO233_R	5´-CTC GCG ACT CGT GGG AAA ATG GGC GGA AGG GCA C C GTG GGA AAA TAG TTC-3´ (RBP-J binding sites underlinded)	

673

674

675 **Table S2.** Constructs cloned by PCR.

Plasmid	**Template**	**Primer Forward**	**Primer Reverse**	**Enzymes**	**Ligation**
pMIGR1 pSV40-Puro	pLXSPHAMel18 ATG	Puro EcoRI F	Puro HindIII R	EcoRI/ HindIII	pMIGRI IRES-GFP
pcDNA3.1.Flag -2-mRBPJ	pcDNA3.1.Flag-2-mRBPJ	mRBP_VP16_F	mRBP-TAA_R	PshAI/XhoI	pcDNA3.1.Flag -2-mRBPJΔstop
pcDNA3.1.Flag -2-mRBPJΔstop	pFA-CMV	VP16_XhoI_F	VP16_XbaI_R	XhoI/XbaI	pcDNA3.1-Flag-2-mRBPJ-VP16
pFA-CMV	pcDNA3.1_HisC _MINT_2776-2833	Gal-Mint_F	Gal-Mint_R	BamHI/XbaI	pFA-CMV-Mint-2776-2833(wt)
pMY-Bio-IRES-Blasticidin	pMSCV-FLAG-hRBP-J Ires Blasticidin	Blasticidin NotI fw	Blasticidin SalI rev	NotI/SalI	pMY BioTip60 IRES-GFP

676

677

678 **Figure Legends**

679 **Figure 1.** Overview of Notch signaling**.** (A) Notch signaling occurs between neighboring cells, in
680 which extracellular Notch-DSL interactions initiate signaling, resulting in the cleavage of Notch
681 and release of its intracellular domain (NICD) from the cell membrane that subsequently transits
682 to the nucleus. In the absence of Notch signaling, CSL can bind corepressors (CoR) to repress
683 transcription from Notch target genes. Upon pathway activation, NICD and Mastermind (MAM)
684 form a ternary complex with CSL that activates transcription from Notch target genes. (B)
685 Structure of the CSL-NICD-MAM ternary complex bound to DNA (PDB ID: 2FO1). The structural
686 core of CSL is composed of three domains: NTD (N-terminal domain), BTD (β-trefoil domain),
687 and CTD (C-terminal domain), which are colored cyan, green, and orange, respectively. A β-
688 strand that makes hydrogen-bonding interactions with all three domains is colored magenta.
689 The RAM and ANK domains of NICD are colored yellow and blue, respectively. MAM and DNA
690 are colored red and light pink/blue, respectively. (C) Domain schematics of CSL, NICD, and
691 MAM are colored similarly to the structure. SHARP is a multidomain transcriptional coregulator
692 that contains N-terminal RRM (RNA Recognition Motif) domains, multiple NLS (Nuclear
693 Localization Sequence), a RID (Receptor Interaction Domain), a RBPID (RBPJ Interacting
694 Domain), and a C-terminal SPOC (Spen Paralog and Ortholog C-terminal) domain.

695

696 **Figure 2**. X-ray structure of the RBPJ-SHARP corepressor complex bound to DNA. (A) Ribbon
697 diagram of RBPJ-SHARP-DNA complex with the NTD, BTD, and CTD of RBPJ colored cyan,
698 green, and orange, respectively. SHARP is colored purple, and the DNA is colored light pink
699 and light blue. Magnified views of the interaction of SHARP with the CTD (top) and BTD
700 (bottom) of RBPJ. RBPJ is represented as a molecular surface with CTD and BTD residues that
701 contact SHARP colored orange and green, respectively. The ribbon diagram of SHARP is
702 colored purple with the side chains of SHARP that contact either the BTD or CTD shown as

703 sticks. SHARP residues that were mutated and tested for activity in this study are labeled. (B)
704 Open book representation of RBPJ-SHARP interfaces. (Left) Ribbon diagram with transparent
705 surface of the CTD-SHARP interface, and (right), ribbon diagram with transparent surface of the
706 BTD-SHARP interface. Side chains in RBPJ and SHARP that contribute to the interface are
707 shown. Key residues at the interface that were mutated and tested for activity in this study are
708 labeled. (C) Conformational changes in the CTD of RBPJ as a result of SHARP binding. (Left)
709 Magnified view of the CTD-SHARP complex with labeled secondary structural elements of the
710 CTD. The R438-E2786 salt bridge is also shown. (Middle) Structural overlay of RBPJ (bound)
711 from RBPJ-SHARP complex with an unbound structure of RBPJ (PDBID: 3IAG). The RBPJ
712 bound and unbound structures are colored orange and yellow, respectively. RBPJ residue
713 W441, which undergoes a large conformational change in the bound structure to accommodate
714 the R438-E2786 salt bridge, is shown in both structures. (Right) Ribbon diagram of the unbound
715 RBPJ structure 3IAG.
716
717 **Figure 3**. Comparison of coregulator binding sites on RBPJ. (A) Both SHARP and NICD bind
718 the BTD and CTD of RBPJ. (Left) RBPJ/SHARP/DNA complex structure with RBPJ represented
719 as a gray molecular surface, SHARP as a ribbon diagram colored purple, and the DNA as CPK
720 colored light blue and pink. The RBPJ residues that contact SHARP in the BTD and CTD are
721 colored green and orange, respectively. (Right) LAG-1/NICD/MAM/DNA complex structure
722 (PDBID: 2FO1) with LAG-1 (*C. elegans* CSL ortholog) represented as a gray molecular surface.
723 NICD is represented as a ribbon diagram with its RAM and ANK domains colored yellow and
724 blue, respectively. MAM is depicted as a ribbon diagram and colored red. The DNA is
725 represented in CPK and colored light blue and pink. RBPJ residues that contact RAM in the
726 BTD are colored green and residues that contact ANK in the CTD are colored orange. (B)
727 Structural alignment of SHARP and other coregulators that bind the BTD of CSL. (Left) The
728 BTD of RBPJ is represented as a green molecular surface. SHARP, the RAM domain from LIN-

729 12, RITA1 and FHL1 are colored purple, yellow, light pink, and gray, respectively. The
730 hydrophobic tetrapeptide (ϕWϕP) is labeled. (Right) Sequence alignment of coregulators that
731 bind the BTD of CSL, including the RAM domains of Notch from mammals, *D. melanogaster*,
732 and *C. elegans*, and the corepressors RITA1, FHL1, and SHARP. The conserved ϕWϕP, which
733 is absent in SHARP, is boxed in green. Other conserved regions in RAM that contribute to BTD
734 binding are highlighted, including the basic region (blue), the -HG- motif (orange), and the -GF-
735 motif (magenta). Structurally similar residues in SHARP that align with other BTD binders are
736 boxed and highlighted in gray. (C) Structural similarity of RBPJ-SHARP and Su(H)-Hairless
737 corepressor complexes. Despite no sequence similarity, both SHARP and Hairless bind the
738 CTD in a structurally analogous manner. RBPJ and Su(H) are represented as a gray molecular
739 surface with the SHARP and Hairless binding sites colored orange. SHARP and Hairless are
740 shown as ribbon diagrams and colored purple and yellow, respectively. The DNA is shown as
741 CPK spheres and colored light blue and light pink.
742
743 **Figure 4**. Evolution of coregulator binding sites on CSL. (A) Structural comparison of the CTD
744 of RBPJ with the RHR-C domain of NFAT. The ribbon diagram of the RBPJ-SHARP complex is
745 colored similarly as in Figure 2, whereas NFAT is colored green. The NFAT β-strand βa', which
746 is absent in the CTD of RBPJ, but occupied by SHARP in the complex structure, is labeled. (B)
747 Structural alignment of the BTD from RBPJ with a canonical β-trefoil fold from the ryanodine
748 receptor (RYR). A canonical BTD is composed of 12 β-strands, in which four β-strands are
749 arranged in a pseudo-threefold symmetrical arrangement. The atypical BTD of CSL is missing
750 two of the 12 β-strands that compose a canonical BTD. The RAM domain of NICD acts as a
751 structural surrogate, binding the region left absent by the missing β-strands. The BTD of CSL
752 and RYR are colored green and light pink, respectively. The two β-strands that are missing in

753 the CSL BTD fold are colored light blue and highlighted with red arrowheads. The RAM domain
754 of NICD is colored yellow.
755
756 **Figure 5**. ITC binding analysis of RBPJ and SHARP structure based mutants. Figure shows
757 representative thermograms (raw heat signal and nonlinear least squares fit to the integrated
758 data) for RBPJ binding to SHARP. Each experiment was performed at 25°C, with 40 titrations of
759 7 µl injections spaced 120 s apart. The dissociation constants (K_d) shown for each experiment
760 are indicated in Tables 2 and 3. (A) Native RBPJ and SHARP form a high affinity 1:1 complex
761 with a 5 nM dissociation constant. The SHARP mutants L2791A (C), Y2793A (D), and I2811A
762 (F) have the strongest effect on RBPJ-SHARP complex formation, whereas SHARP mutants
763 V2789A (B) and K2807A (E) only modestly affect RBPJ binding. The RBPJ BTD mutants F261A
764 (G) and A284V (H), and the CTD mutant L388A (I), strongly affect binding to SHARP.
765
766 **Figure 6**. Characterization of RBPJ and SHARP structure based mutants in cells. (A)
767 Coimmunoprecipitation (CoIP) of RBPJ with wild-type and mutant SHARP constructs. HEK293
768 cells were cotransfected with GFP-SHARP (2766-2833), which corresponds to the RBPJ-
769 interaction-domain of SHARP (RBPID), and Flag-RBPJ. Expression of GFP-SHARP (middle
770 panel) and Flag-RBPJ (bottom panel) proteins was verified by Western blotting. CoIPs were
771 performed 24h after transfection. The asterisk denotes the heavy chain of anti-Flag antibody
772 used for immunoprecipitation. (B) CoIP of SHARP with wild-type and mutant RBPJ constructs.
773 HEK293 cells were cotransfected with GFP-RBPJ and Flag-SHARP (RBPID). Expression of
774 Flag-SHARP (middle panel) and GFP-RBPJ (bottom panel) proteins was verified by Western
775 blotting. CoIPs were performed 24h after transfection. The asterisk denotes the heavy chain of
776 anti-Flag antibody used for immunoprecipitation. (C-D) Analysis of structure based SHARP and
777 RBPJ mutants using a mammalian two-hybrid assay. HeLa cells were cotransfected with the
778 indicated Gal4-SHARP (300ng) and RBPJ-VP16 (150ng) constructs together with the pFR-Luc

779 reporter (500ng), which contains five Gal4 DNA binding sites upstream of the luciferase gene.
780 Relative luciferase activity was determined after cotransfection of the pFR-Luc reporter
781 construct alone. Mean values and standard deviations are from at least six independent
782 experiments. (E) Control experiments showing RBPJ-VP16 mutants are competent to bind and
783 activate reporter similar to wild-type. HeLa cells were cotransfected with RBPJ-VP16 constructs
784 (150ng) and the 12xCSL-RE luciferase reporter (500ng), which contains 12 CSL DNA binding
785 sites upstream of the luciferase gene. Relative luciferase activity was determined after
786 cotransfection of the reporter construct alone. Mean values and standard deviations are from
787 four independent experiments [***P < 0.001, (ns) not significant, unpaired student´s *t*-test].
788
789 **Figure 7**. The RBPJ-SHARP interaction is required for repression of Notch target genes in cells.
790 (A) The wild-type SHARP RBPID ($RBPID^{WT}$), but not the RBPJ-interacting defective SHARP
791 RBPID ($RBPID^{LI/AA}$) mutant, causes upregulation of Notch target genes in mouse mature T (MT)
792 cells by outcompeting endogenous SHARP for RBPJ binding. MT cells were infected with
793 plasmids encoding GFP-tagged SHARP (2776-2833), either wild-type (GFP-SHARP/$RBPID^{WT}$,
794 black bars) or the RBPJ-interacting defective mutant L2791A/I2811A (GFP-SHARP/$RBPID^{LI/AA}$,
795 gray bars), or an empty vector control (Control, white bars). (Left) Total RNA from MT cells
796 infected with plasmids encoding GFP-SHARP/$RBPID^{WT}$, GFP-SHARP/$RBPID^{LI/AA}$, or an empty
797 vector control, were reverse transcribed into cDNA and analyzed by qPCR using primers
798 specific for *Tbp*, *Hes1* or *Hey1*. Data were normalized to the housekeeping gene *GusB*
799 (glucuronidase β). Data shown represent the mean ± SD of triplicate experiments ([**] P < 0.01,
800 [***] P < 0.001, unpaired Student's *t*-test). (Right) Nuclear extracts (NE) were prepared from MT
801 cells infected with GFP-SHARP/$RBPID^{WT}$, GFP-SHARP/$RBPID^{LI/AA}$, or an empty vector control
802 and analyzed by Western blotting using a GFP antibody and with TBP used as a loading
803 control. (B) RBPJ is required to repress Notch target genes *Hes1* and *Hey1* in MT cells as
804 revealed by CRISPR/Cas9 depletion of RBPJ. (Left) Total RNA from wild-type (*Control*) or

805 RBPJ depleted (clones *sgRbpj 2-12* and *sgRbpj 2-14*) MT cells was reverse transcribed into
806 cDNA and analyzed by qPCR using primers specific for *Tbp*, *Hes1* or *Hey1*. Data were
807 normalized to the housekeeping gene *GusB* (*glucuronidase* β). Shown is the mean ± SD of
808 triplicate experiments ([*] P < 0.05, [**] P < 0.01, [***] P < 0.001, unpaired Student's *t*-test).
809 (Right) Whole cell extracts (WCE) were prepared from wild-type (*Control*) or RBPJ depleted
810 (clones *sgRbpj 2-12* and *sgRbpj 2-14*) MT cells and analyzed by Western blotting using an anti-
811 RBPJ antibody. GAPDH was used as loading control. (C) *Hes1* and *Hey1* Notch target genes
812 are upregulated upon shRNA-mediated *Rbpj* knockdown, but not with the *SCR* control shRNA.
813 (Left) Total RNA from MT cells infected with shRNAs targeting *Rbpj* (*Rbpj sh1* or *Rbpj sh4*) or
814 scrambled shRNA control (SCR) was reverse transcribed into cDNA and analyzed by qPCR
815 using primers specific for *Tbp*, *Hes1* or *Hey1*. Data were normalized to the housekeeping gene
816 *GusB* (*glucuronidase* β). Shown is the mean ± SD of quadruplicate experiments ([**] P < 0.01,
817 [***] P < 0.001, unpaired Student's *t*-test). (Right) WCE was prepared from MT cells infected
818 with shRNAs targeting *Rbpj* (*Rbpj sh1* or *Rbpj sh4*) or a scrambled shRNA control (*SCR*) and
819 analyzed by Western blotting using a RBPJ antibody. GAPDH was used as loading control. (D)
820 Expression of wild-type RBPJ ($RBPJ^{WT}$), but not the SHARP-interacting defective mutant
821 F261A/L388A ($RBPJ^{FL/AA}$), in the RBPJ-depleted background rescues the repression of Notch
822 target genes. (Left) Total RNA from *sgRbpj 2-12* MT cells infected with empty vector (Control),
823 $RBPJ^{WT}$ or $RBPJ^{FL/AA}$ was reverse transcribed into cDNA and analyzed by qPCR using primers
824 specific for *Tbp*, *Hes1* or *Hey1*. Data were normalized to the housekeeping gene *GusB*
825 (*glucuronidase* β). Shown is the mean ± SD of three independent experiments measured twice
826 each ([*] P < 0.05, [**] P < 0.01, [***] P < 0.001, unpaired Student's *t*-test). (Right) NEs were
827 prepared from *sgRbpj 2-12* MT cells infected with empty vector (Control), $RBPJ^{WT}$ or $RBPJ^{FL/AA}$
828 and analyzed by Western blotting using anti-RBPJ antibodies. Histone H3 was used as a
829 loading control.

830

831 **Figure S1.** Composition and analysis of the asymmetric unit of the RBPJ/MBP-SHARP/DNA
832 complex crystals. (A) The asymmetric unit of the RBPJ/MBP-SHARP/DNA complex crystals
833 contains two RBPJ/MBP-SHARP/DNA complexes. RBPJ, MBP, and SHARP are shown as
834 ribbon diagrams and colored green, cyan, and purple, respectively. The DNA is colored gray.
835 (B) ITC thermogram showing the affinity of MBP-SHARP for RBPJ. (C-D) Structural overlays of
836 the two complexes contained within the asymmetric unit of the crystals. (C) Structural alignment
837 overall all cα atoms. (D) Resulting structural overlay when only RBPJ cα atoms are aligned. (E)
838 Resulting structural overlay when only MBP cα atoms are aligned. (F) Resulting structural
839 overlay when only SHARP cα atoms are aligned. Red arrows highlight the large conformational
840 differences in the poorly ordered linkers of SHARP that lie between the regions that bind the
841 BTD and CTD of RBPJ.

842

843 **Figure S2.** Control studies of the structure based RBPJ mutants. (A) Differential scanning
844 fluorimetry (DSF) was used to analyze the melting temperatures (Tm) of wild-type and mutant
845 RBPJ proteins. Figure shows melt curve and derivative plot. Tm determined for wild-type and
846 mutant RBPJ proteins is the mean ± SD of experiments performed in triplicate. (B) Upper
847 panel, analysis of DNA binding by EMSA of wild-type RBPJ and select RBPJ mutants.
848 Oligomeric duplex DNA probe used in EMSA 5´-
849 CCTGGAACTATT**TTCCCACG**GTGCCCTTCCGCCCATT**TTCCCACG**AGTCG-3´ with RBPJ
850 binding sites in bold and underlined. The DNA interaction bands are labeled A and B. The
851 asterisk denotes a nonspecific background band. Addition of α-Flag antibodies lead to
852 supershifted Flag-RBPJ/DNA complexes (complexes a and b) in the EMSA, demonstrating
853 specificity. Lower panel,N-terminally tagged Flag-RBPJ fusion proteins were translated *in vitro*
854 with the TNT T7 coupled Reticulocyte Lysate System Kit (Promega) and relative protein levels

855 were analyzed by Western blotting. Flag-RBPJ/DNA complexes, labeled a and b, were
856 supershifted in the EMSA using α-Flag antibodies, demonstrating specificity. (C) Subcellular
857 localization of RBPJ proteins after expression in HeLa cells. HeLa cells were transiently
858 transfected with 0.3 µg of the respective plasmids GFP-RBPJ: WT, F261A, L388A, and
859 F261A/L388A. After 24 h cells were fixed and the images were taken 24 h after transfection with
860 DAPI staining under the fluorescence microscope using a 63x lens. The superimposition (right
861 column) of the DAPI signal (center) with the GFP signal (left) illustrates the predominantly
862 nuclear localization of the RBPJ proteins. (D) NICD binding of wild-type and mutant RBPJ
863 proteins from cells. HEK293 cells were transfected with the plasmids GFP-RBPJ^{WT}, GFP-
864 RBPJ^{F261A} GFP-RBPJ^{L388A}, or GFP-RBPJ$^{F261A/L388A}$ plasmids together with with Flag-NICD (lanes
865 2-6). Immunoprecipitation was performed with the α-Flag antibody agarose beads and detected
866 by Western blotting using an α-GFP antibody. The expression of the Flag-tagged NICD protein
867 (lower blot) could be detected using an α-Flag antibody. The asterisk in the upper blot marks the
868 heavy chain of the antibody used for immunoprecipitation.

869

870 **References**

871 1 Kovall, R. A., Gebelein, B., Sprinzak, D. & Kopan, R. The Canonical Notch Signaling Pathway:
872 Structural and Biochemical Insights into Shape, Sugar, and Force. *Dev Cell* **41**, 228-241,
873 doi:10.1016/j.devcel.2017.04.001 (2017).
874 2 Bray, S. J. Notch signalling in context. *Nat Rev Mol Cell Biol* **17**, 722-735,
875 doi:10.1038/nrm.2016.94 (2016).
876 3 Siebel, C. & Lendahl, U. Notch Signaling in Development, Tissue Homeostasis, and Disease.
877 *Physiological reviews* **97**, 1235-1294, doi:10.1152/physrev.00005.2017 (2017).
878 4 Braune, E. B. & Lendahl, U. Notch -- a goldilocks signaling pathway in disease and cancer
879 therapy. *Discovery medicine* **21**, 189-196 (2016).
880 5 Ntziachristos, P., Lim, J. S., Sage, J. & Aifantis, I. From fly wings to targeted cancer therapies: a
881 centennial for notch signaling. *Cancer cell* **25**, 318-334, doi:10.1016/j.ccr.2014.02.018 (2014).
882 6 Kovall, R. A. & Blacklow, S. C. Mechanistic insights into Notch receptor signaling from structural
883 and biochemical studies. *Curr Top Dev Biol* **92**, 31-71, doi:S0070-2153(10)92002-4 [pii]

884 10.1016/S0070-2153(10)92002-4 (2010).
885 7 Borggrefe, T. & Oswald, F. The Notch signaling pathway: transcriptional regulation at Notch
886 target genes. *Cell Mol Life Sci* **66**, 1631-1646 (2009).

887 8 Kuroda, K. *et al.* Regulation of marginal zone B cell development by MINT, a suppressor of
888 Notch/RBP-J signaling pathway. *Immunity* **18**, 301-312 (2003).
889 9 Oswald, F. *et al.* SHARP is a novel component of the Notch/RBP-Jkappa signalling pathway. *Embo*
890 *J* **21**, 5417-5426 (2002).
891 10 Maier, D. Hairless: the ignored antagonist of the Notch signalling pathway. *Hereditas* **143**, 212-
892 221, doi:10.1111/j.2007.0018-0661.01971.x (2006).
893 11 Taniguchi, Y., Furukawa, T., Tun, T., Han, H. & Honjo, T. LIM protein KyoT2 negatively regulates
894 transcription by association with the RBP-J DNA-binding protein. *Mol Cell Biol* **18**, 644-654
895 (1998).
896 12 Xu, T. *et al.* RBPJ/CBF1 interacts with L3MBTL3/MBT1 to promote repression of Notch signaling
897 via histone demethylase KDM1A/LSD1. *EMBO J* **36**, 3232-3249, doi:10.15252/embj.201796525
898 (2017).
899 13 Tabaja, N., Yuan, Z., Oswald, F. & Kovall, R. A. Structure-function analysis of RBP-J-interacting
900 and tubulin-associated (RITA) reveals regions critical for repression of Notch target genes. *J Biol*
901 *Chem* **292**, 10549-10563, doi:10.1074/jbc.M117.791707 (2017).
902 14 Wacker, S. A. *et al.* RITA, a novel modulator of Notch signalling, acts via nuclear export of RBP-J.
903 *Embo J* **30**, 43-56, doi:emboj2010289 [pii]

904 10.1038/emboj.2010.289 (2011).
905 15 Wilson, J. J. & Kovall, R. A. Crystal structure of the CSL-Notch-Mastermind ternary complex
906 bound to DNA. *Cell* **124**, 985-996, doi:10.1016/j.cell.2006.01.035 (2006).
907 16 Nam, Y., Sliz, P., Song, L., Aster, J. C. & Blacklow, S. C. Structural basis for cooperativity in
908 recruitment of MAML coactivators to Notch transcription complexes. *Cell* **124**, 973-983,
909 doi:10.1016/j.cell.2005.12.037 (2006).
910 17 Kovall, R. A. & Hendrickson, W. A. Crystal structure of the nuclear effector of Notch signaling,
911 CSL, bound to DNA. *EMBO J* **23**, 3441-3451, doi:10.1038/sj.emboj.7600349 (2004).
912 18 Yuan, Z. *et al.* Structure and Function of the Su(H)-Hairless Repressor Complex, the Major
913 Antagonist of Notch Signaling in Drosophila melanogaster. *PLoS Biol* **14**, e1002509,
914 doi:10.1371/journal.pbio.1002509 (2016).
915 19 Collins, K. J., Yuan, Z. & Kovall, R. A. Structure and function of the CSL-KyoT2 corepressor
916 complex: a negative regulator of Notch signaling. *Structure* **22**, 70-81,
917 doi:10.1016/j.str.2013.10.010 (2014).
918 20 Shi, Y. *et al.* Sharp, an inducible cofactor that integrates nuclear receptor repression and
919 activation. *Genes Dev* **15**, 1140-1151, doi:10.1101/gad.871201 (2001).
920 21 Newberry, E. P., Latifi, T. & Towler, D. A. The RRM domain of MINT, a novel Msx2 binding
921 protein, recognizes and regulates the rat osteocalcin promoter. *Biochemistry* **38**, 10678-10690,
922 doi:10.1021/bi990967j (1999).
923 22 Salat, D., Liefke, R., Wiedenmann, J., Borggrefe, T. & Oswald, F. ETO, but not leukemogenic
924 fusion protein AML1/ETO, augments RBP-Jkappa/SHARP-mediated repression of notch target
925 genes. *Mol Cell Biol* **28**, 3502-3512, doi:10.1128/MCB.01966-07 (2008).
926 23 Oswald, F. *et al.* RBP-Jkappa/SHARP recruits CtIP/CtBP corepressors to silence Notch target
927 genes. *Mol Cell Biol* **25**, 10379-10390, doi:10.1128/MCB.25.23.10379-10390.2005 (2005).
928 24 Oswald, F. *et al.* A phospho-dependent mechanism involving NCoR and KMT2D controls a
929 permissive chromatin state at Notch target genes. *Nucleic Acids Res* **44**, 4703-4720 (2016).
930 25 McHugh, C. A. *et al.* The Xist lncRNA interacts directly with SHARP to silence transcription
931 through HDAC3. *Nature* **521**, 232-236, doi:10.1038/nature14443 (2015).
932 26 Chu, C. *et al.* Systematic discovery of Xist RNA binding proteins. *Cell* **161**, 404-416,
933 doi:10.1016/j.cell.2015.03.025 (2015).

934 27 VanderWielen, B. D., Yuan, Z., Friedmann, D. R. & Kovall, R. A. Transcriptional repression in the
935 Notch pathway: thermodynamic characterization of CSL-MINT (Msx2-interacting nuclear target
936 protein) complexes. *J Biol Chem* **286**, 14892-14902, doi:10.1074/jbc.M110.181156 (2011).
937 28 Moon, A. F., Mueller, G. A., Zhong, X. & Pedersen, L. C. A synergistic approach to protein
938 crystallization: combination of a fixed-arm carrier with surface entropy reduction. *Protein Sci* **19**,
939 901-913, doi:10.1002/pro.368 (2010).
940 29 Choi, S. H. *et al.* Conformational locking upon cooperative assembly of notch transcription
941 complexes. *Structure* **20**, 340-349, doi:10.1016/j.str.2011.12.011 (2012).
942 30 Friedmann, D. R., Wilson, J. J. & Kovall, R. A. RAM-induced allostery facilitates assembly of a
943 notch pathway active transcription complex. *J Biol Chem* **283**, 14781-14791, doi:M709501200
944 [pii]

945 10.1074/jbc.M709501200 (2008).
946 31 Johnson, S. E., Ilagan, M. X., Kopan, R. & Barrick, D. Thermodynamic analysis of the CSL x Notch
947 interaction: distribution of binding energy of the Notch RAM region to the CSL beta-trefoil
948 domain and the mode of competition with the viral transactivator EBNA2. *J Biol Chem* **285**,
949 6681-6692, doi:10.1074/jbc.M109.019968 (2010).
950 32 Del Bianco, C., Aster, J. C. & Blacklow, S. C. Mutational and energetic studies of Notch 1
951 transcription complexes. *J Mol Biol* **376**, 131-140, doi:S0022-2836(07)01560-4 [pii]

952 10.1016/j.jmb.2007.11.061 (2008).
953 33 Lubman, O. Y., Ilagan, M. X., Kopan, R. & Barrick, D. Quantitative dissection of the Notch:CSL
954 interaction: insights into the Notch-mediated transcriptional switch. *J Mol Biol* **365**, 577-589,
955 doi:10.1016/j.jmb.2006.09.071 (2007).
956 34 Maier, D. *et al.* Structural and functional analysis of the repressor complex in the Notch signaling
957 pathway of Drosophila melanogaster. *Mol Biol Cell* **22**, 3242-3252, doi:mbc.E11-05-0420 [pii]

958 10.1091/mbc.E11-05-0420 (2011).
959 35 Kurth, P., Preiss, A., Kovall, R. A. & Maier, D. Molecular analysis of the notch repressor-complex
960 in Drosophila: characterization of potential hairless binding sites on suppressor of hairless. *PLoS*
961 *One* **6**, e27986, doi:10.1371/journal.pone.0027986

962 PONE-D-11-18755 [pii] (2011).
963 36 Yuan, Z., Friedmann, D. R., VanderWielen, B. D., Collins, K. J. & Kovall, R. A. Characterization of
964 CSL (CBF-1, Su(H), Lag-1) mutants reveals differences in signaling mediated by Notch1 and
965 Notch2. *J Biol Chem* **287**, 34904-34916, doi:M112.403287 [pii]

966 10.1074/jbc.M112.403287 (2012).
967 37 Jung, C., Mittler, G., Oswald, F. & Borggrefe, T. RNA helicase Ddx5 and the noncoding RNA SRA
968 act as coactivators in the Notch signaling pathway. *Biochimica et biophysica acta* **1833**, 1180-
969 1189, doi:10.1016/j.bbamcr.2013.01.032 (2013).
970 38 Bray, S. & Bernard, F. Notch targets and their regulation. *Curr Top Dev Biol* **92**, 253-275,
971 doi:S0070-2153(10)92008-5 [pii]

972 10.1016/S0070-2153(10)92008-5 (2010).
973 39 Surendran, K. *et al.* The contribution of Notch1 to nephron segmentation in the developing
974 kidney is revealed in a sensitized Notch2 background and can be augmented by reducing Mint
975 dosage. *Developmental biology* **337**, 386-395, doi:10.1016/j.ydbio.2009.11.017 (2010).

976 40 Tsuji, M., Shinkura, R., Kuroda, K., Yabe, D. & Honjo, T. Msx2-interacting nuclear target protein
977 (Mint) deficiency reveals negative regulation of early thymocyte differentiation by Notch/RBP-J
978 signaling. *Proc Natl Acad Sci USA* **104**, 1610-1615, doi:10.1073/pnas.0610520104 (2007).
979 41 Chan, S. K. K. *et al.* Role of co-repressor genomic landscapes in shaping the Notch response. *PLoS*
980 *genetics* **13**, e1007096, doi:10.1371/journal.pgen.1007096 (2017).
981 42 Castel, D. *et al.* Dynamic binding of RBPJ is determined by Notch signaling status. *Genes Dev* **27**,
982 1059-1071, doi:10.1101/gad.211912.112 (2013).
983 43 Kao, H. Y. *et al.* A histone deacetylase corepressor complex regulates the Notch signal
984 transduction pathway. *Genes Dev* **12**, 2269-2277 (1998).
985 44 Hsieh, J. J. & Hayward, S. D. Masking of the CBF1/RBPJ kappa transcriptional repression domain
986 by Epstein-Barr virus EBNA2. *Science* **268**, 560-563 (1995).
987 45 Torella, R. *et al.* A combination of computational and experimental approaches identifies DNA
988 sequence constraints associated with target site binding specificity of the transcription factor
989 CSL. *Nucleic Acids Res* **42**, 10550-10563, doi:10.1093/nar/gku730 (2014).
990 46 Friedmann, D. R. & Kovall, R. A. Thermodynamic and structural insights into CSL-DNA complexes.
991 *Protein Sci* **19**, 34-46, doi:10.1002/pro.280 (2010).
992 47 Gomez-Lamarca, M. J. *et al.* Activation of the Notch Signaling Pathway In Vivo Elicits Changes in
993 CSL Nuclear Dynamics. *Dev Cell* **44**, 611-623 e617, doi:10.1016/j.devcel.2018.01.020 (2018).
994 48 Ariyoshi, M. & Schwabe, J. W. A conserved structural motif reveals the essential transcriptional
995 repression function of Spen proteins and their role in developmental signaling. *Genes Dev* **17**,
996 1909-1920 (2003).
997 49 Zehender, A. *et al.* Conservation of the Notch antagonist Hairless in arthropods: functional
998 analysis of the crustacean Daphnia pulex Hairless gene. *Development genes and evolution* **227**,
999 339-353, doi:10.1007/s00427-017-0593-4 (2017).
1000 50 McCoy, A. J. *et al.* Phaser crystallographic software. *Journal of applied crystallography* **40**, 658-
1001 674, doi:10.1107/S0021889807021206 (2007).
1002 51 Adams, P. D. *et al.* PHENIX: a comprehensive Python-based system for macromolecular structure
1003 solution. *Acta crystallographica. Section D, Biological crystallography* **66**, 213-221,
1004 doi:10.1107/S0907444909052925 (2010).
1005 52 Emsley, P. & Cowtan, K. Coot: model-building tools for molecular graphics. *Acta*
1006 *crystallographica. Section D, Biological crystallography* **60**, 2126-2132 (2004).
1007 53 Smart, O. S. *et al.* Exploiting structure similarity in refinement: automated NCS and target-
1008 structure restraints in BUSTER. *Acta crystallographica. Section D, Biological crystallography* **68**,
1009 368-380, doi:10.1107/S0907444911056058 (2012).
1010 54 Davis, I. W. *et al.* MolProbity: all-atom contacts and structure validation for proteins and nucleic
1011 acids. *Nucleic Acids Res* **35**, W375-383 (2007).
1012 55 Krissinel, E. & Henrick, K. Inference of macromolecular assemblies from crystalline state. *J Mol*
1013 *Biol* **372**, 774-797 (2007).

1014

1015

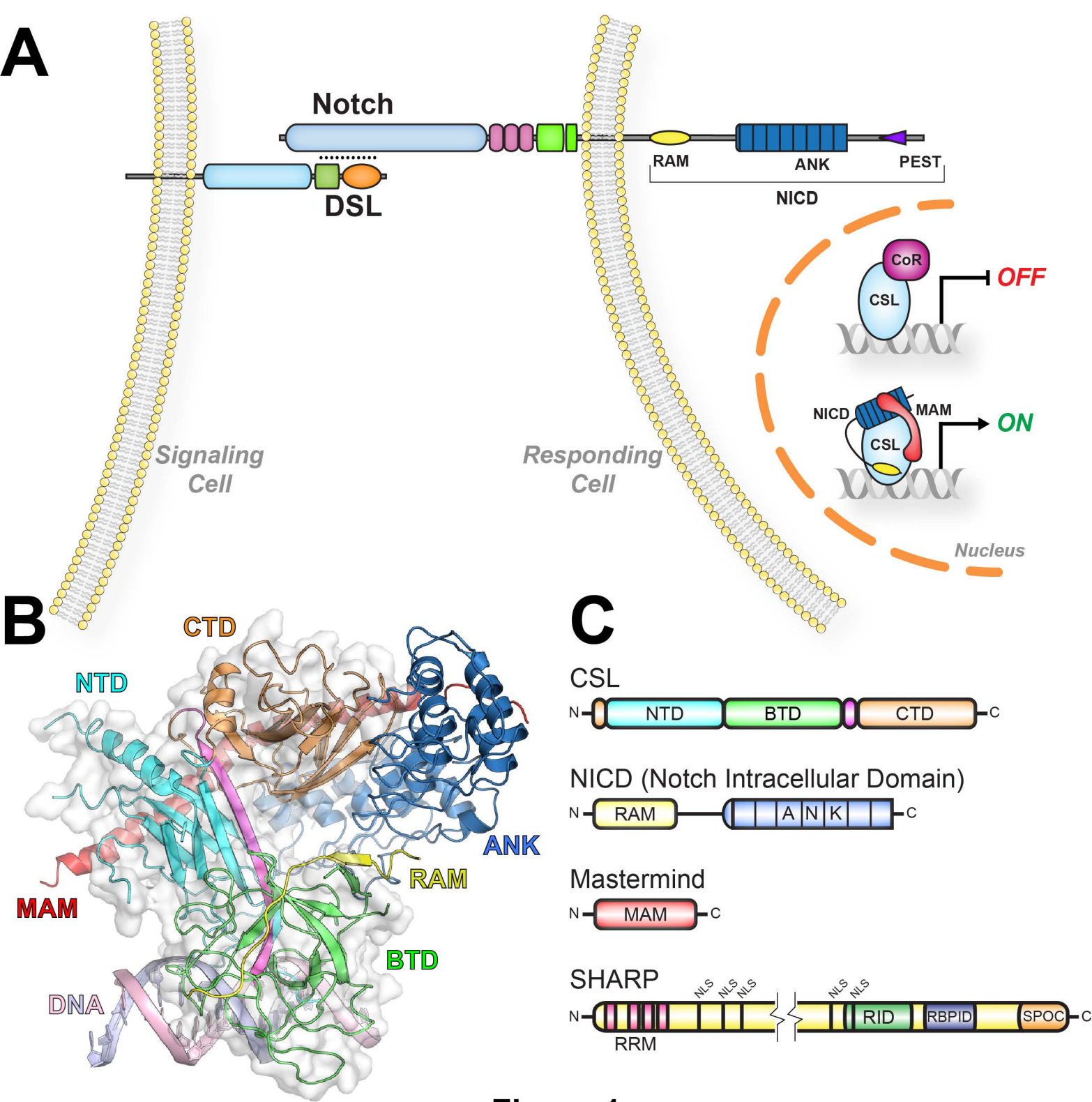
A
Notch
DSL
RAM
ANK
PEST
NICD
CoR
CSL
OFF
NICD
MAM
CSL
ON
Signaling Cell
Responding Cell
Nucleus
B
CTD
NTD
ANK
RAM
MAM
BTD
DNA
C
CSL
N
NTD
BTD
CTD
C
NICD (Notch Intracellular Domain)
N
RAM
A N K
C
Mastermind
N
MAM
C
SHARP
NLS
NLS
NLS
NLS
NLS
N
RID
RBPID
SPOC
C
RRM

Figure 1

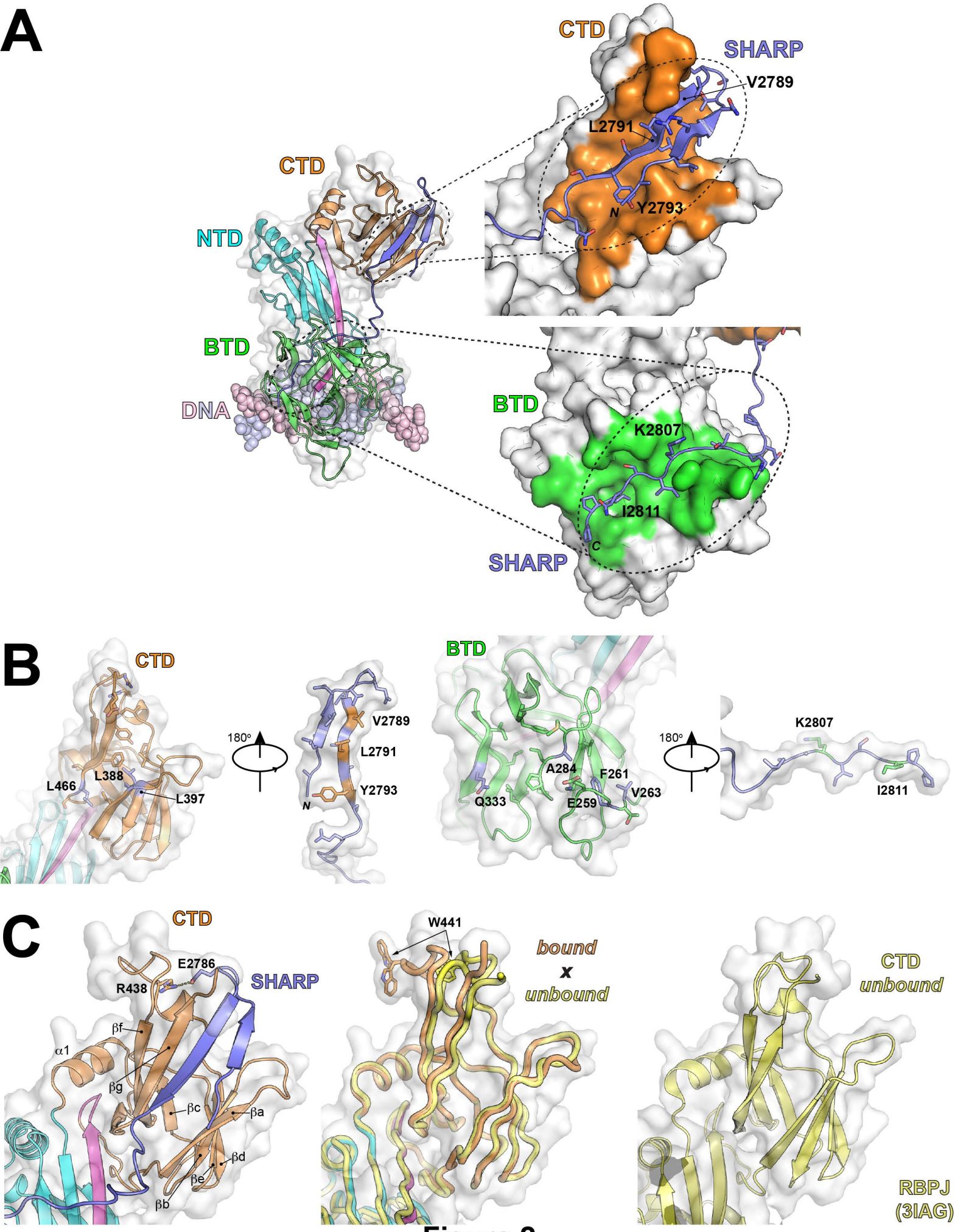
A
CTD
SHARP
V2789
L2791
N
Y2793
CTD
NTD
BTD
DNA
BTD
K2807
I2811
C
SHARP
B
CTD
L466
L388
L397
180°
V2789
L2791
Y2793
N
BTD
A284
F261
Q333
E259
V263
180°
K2807
I2811
C
CTD
E2786
R438
SHARP
βf
α1
βg
βc
βa
βd
βe
βb
W441
bound
x
unbound
CTD
unbound
RBPJ
(3IAG)

Figure 2

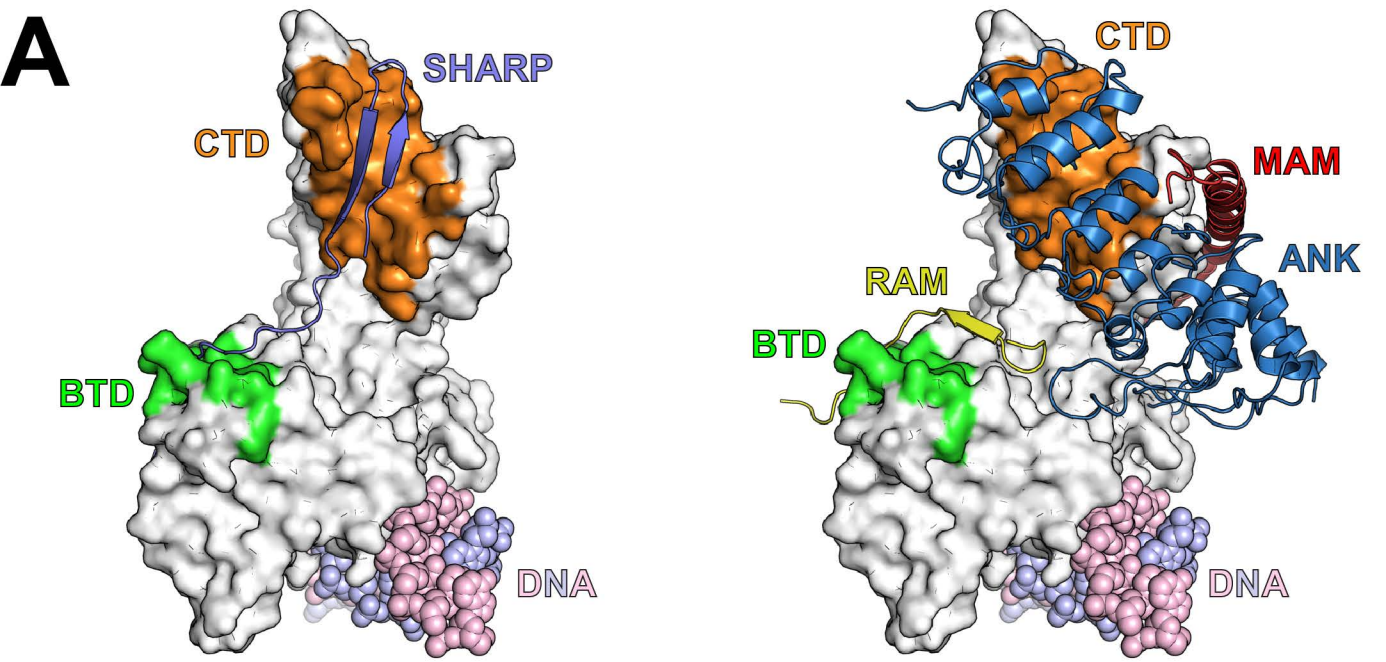

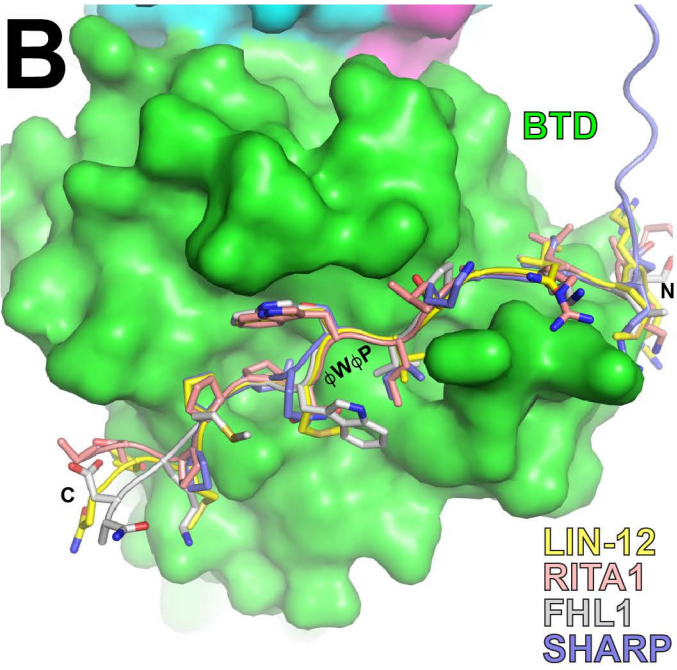

Notch1	R	K	R	R	R	Q	H	G	Q	L	W	F	P	E	G	F	K	V
Notch2	A	K	R	K	R	K	H	G	F	L	W	L	P	E	G	F	T	L
Notch3	A	R	R	K	R	E	H	S	T	L	W	F	P	E	G	F	S	L
Notch4	R	R	R	R	R	E	H	G	A	L	W	L	P	P	G	F	I	R
Notch	T	Q	R	K	R	A	H	G	V	T	W	F	P	E	G	F	R	A
LIN-12	R	K	R	R	M	I	N	A	S	V	W	M	P	P	M	E	N	E
RITA1	G	D	A	A	K	L	R	A	L	L	W	T	P	P	P	T	P	R
FHL1	C	N	K	G	L	V	K	A	P	V	W	W	P	M	K	D	N	P
SHARP			P	Q	R	I	S	A	K	I	S	Q	I	P	P			

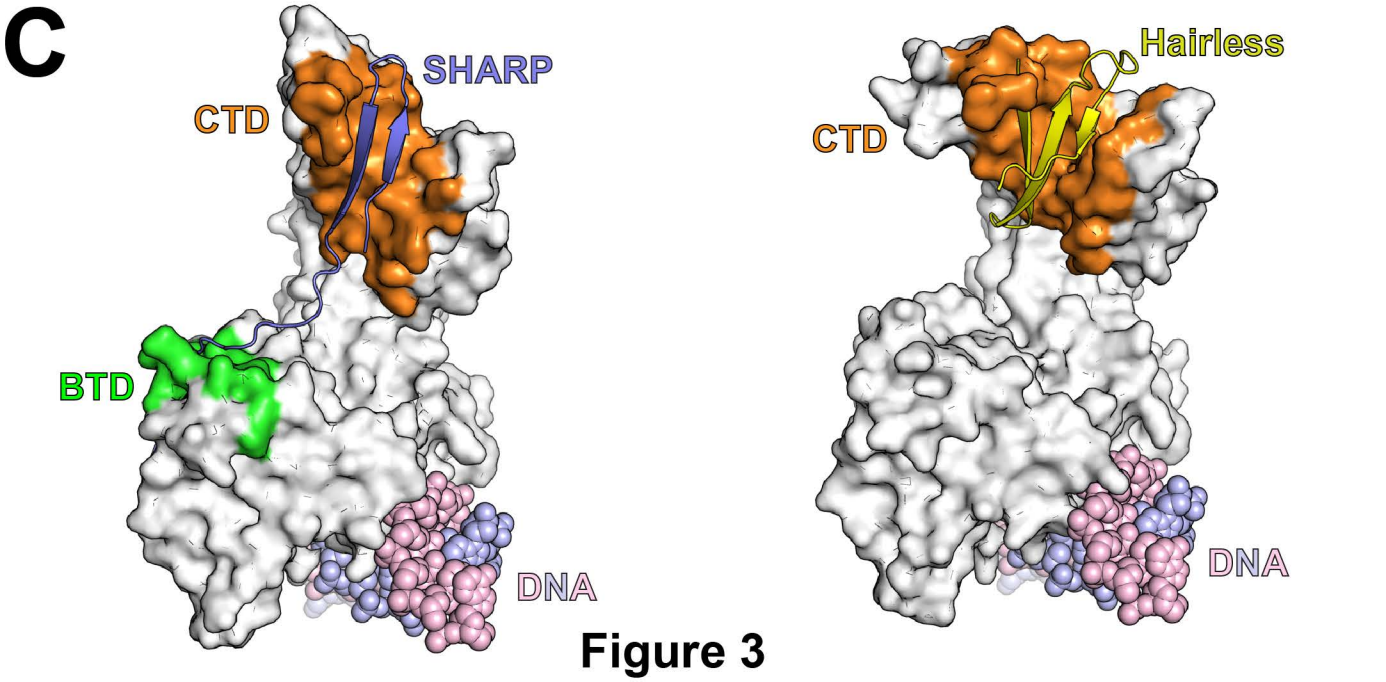

Figure 3

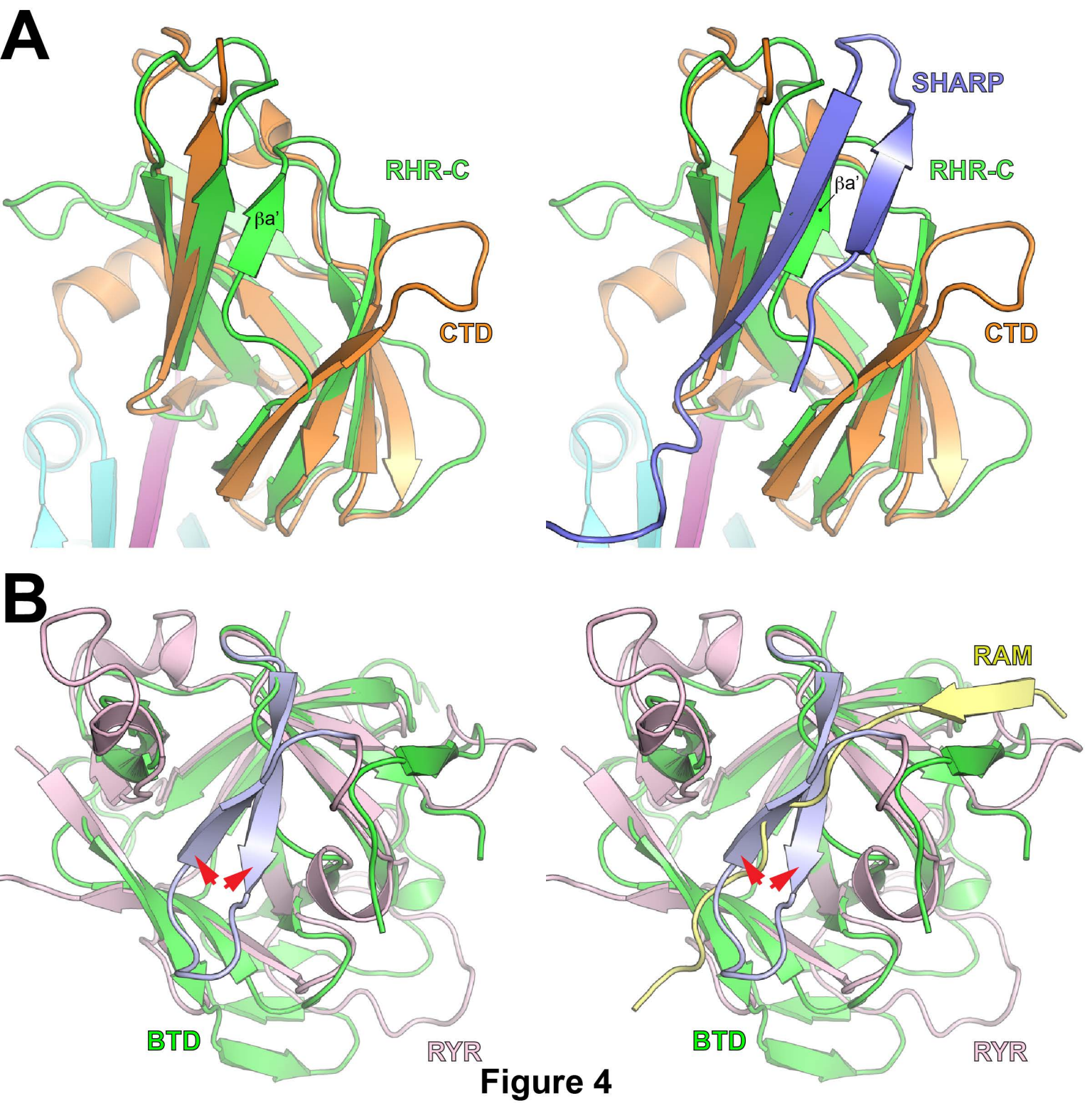

Figure 4

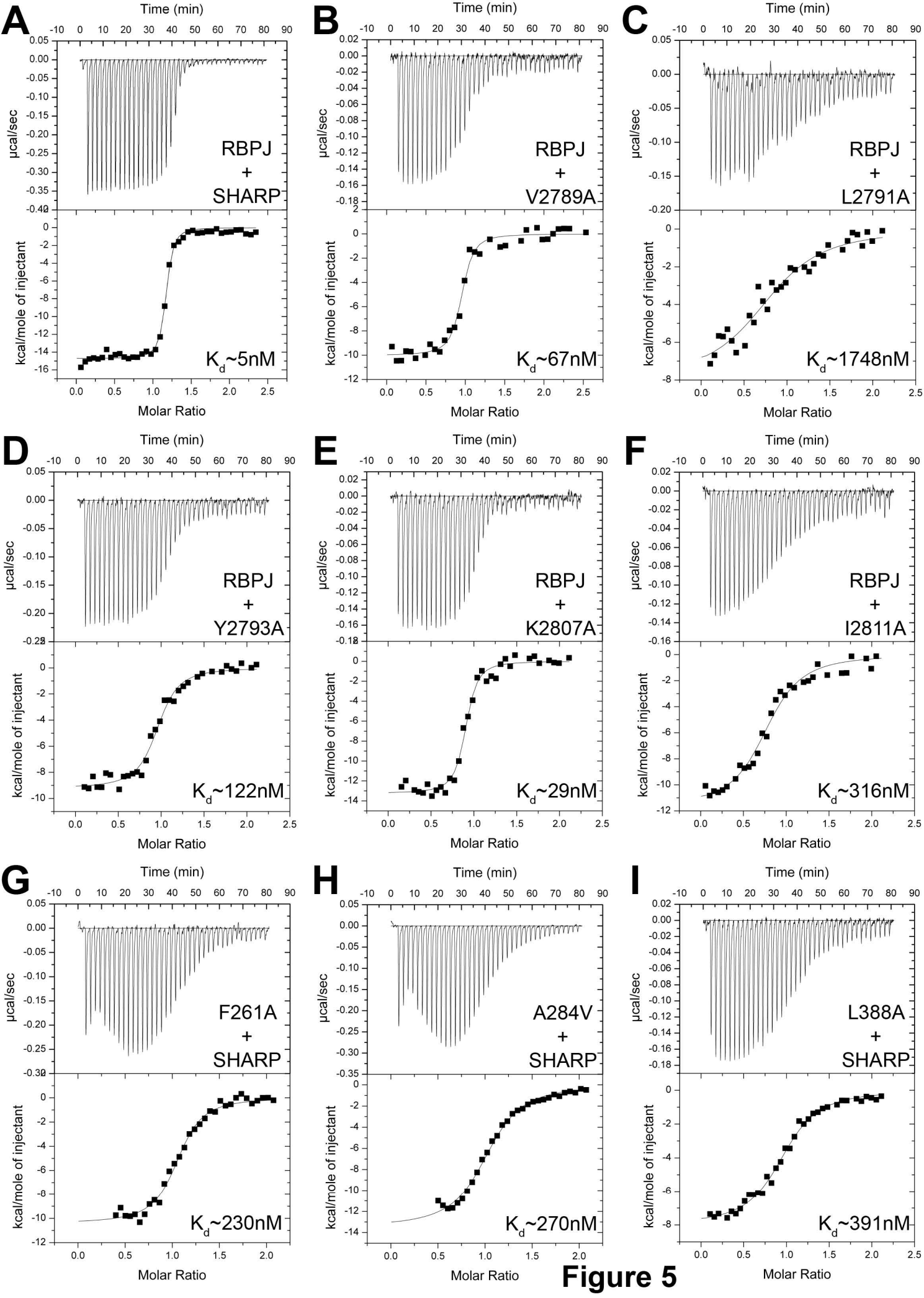
A
Time (min)
µcal/sec
RBPJ
+
SHARP
kcal/mole of injectant
K_d~5nM
Molar Ratio
B
RBPJ
+
V2789A
K_d~67nM
C
RBPJ
+
L2791A
K_d~1748nM
D
RBPJ
+
Y2793A
K_d~122nM
E
RBPJ
+
K2807A
K_d~29nM
F
RBPJ
+
I2811A
K_d~316nM
G
F261A
+
SHARP
K_d~230nM
H
A284V
+
SHARP
K_d~270nM
I
L388A
+
SHARP
K_d~391nM

Figure 5

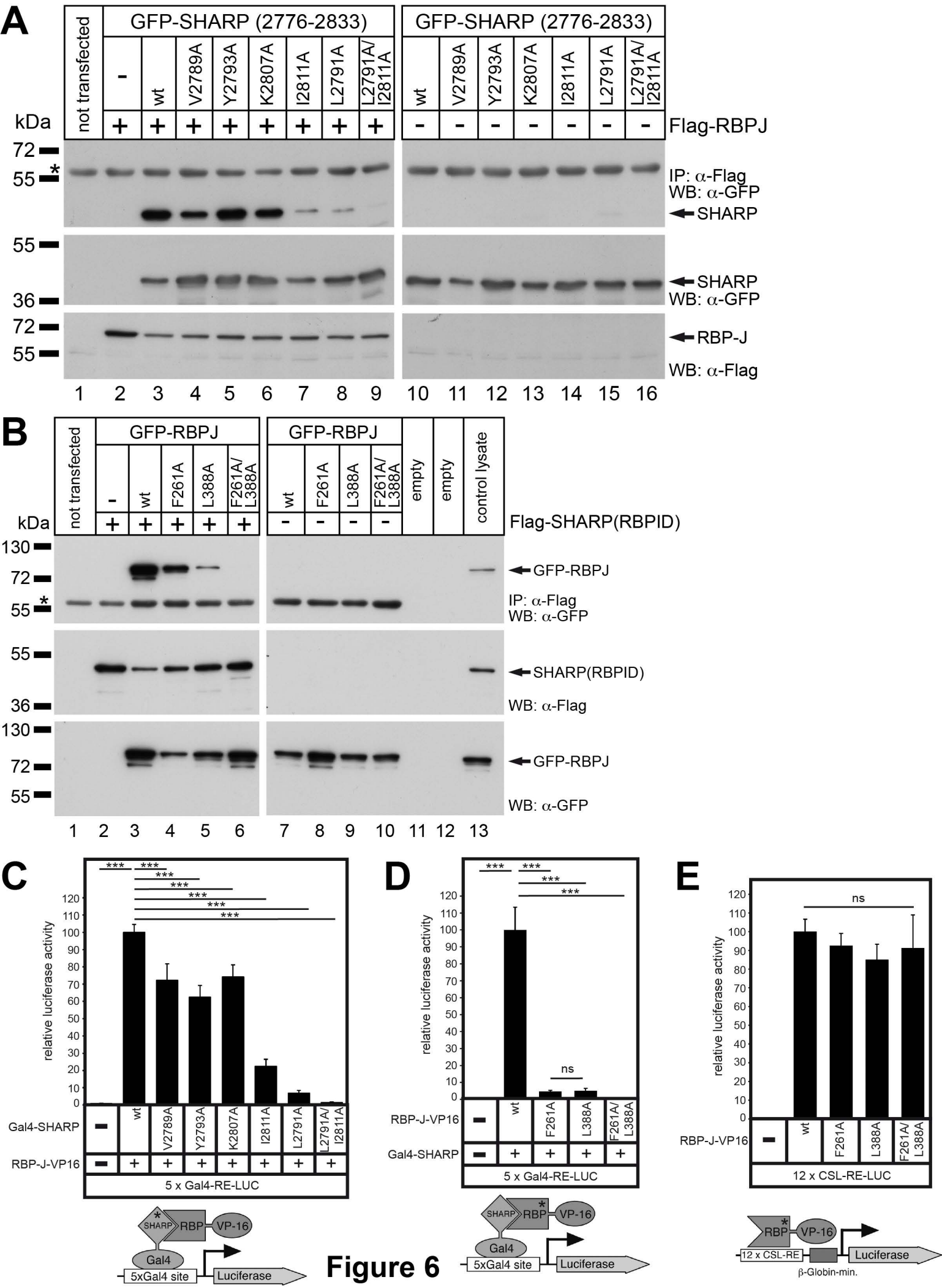
A
not transfected
GFP-SHARP (2776-2833)
-
wt
V2789A
Y2793A
K2807A
I2811A
L2791A
L2791A/ I2811A
kDa
Flag-RBPJ
72
55
*
IP: α-Flag
WB: α-GFP
SHARP
36
WB: α-GFP
RBP-J
WB: α-Flag
1 2 3 4 5 6 7 8 9 10 11 12 13 14 15 16
B
GFP-RBPJ
F261A
L388A
F261A/ L388A
empty
control lysate
Flag-SHARP(RBPID)
130
GFP-RBPJ
SHARP(RBPID)
WB: α-Flag
WB: α-GFP
1 2 3 4 5 6 7 8 9 10 11 12 13
C
relative luciferase activity
Gal4-SHARP
RBP-J-VP16
5 x Gal4-RE-LUC
SHARP
RBP
VP-16
Gal4
5xGal4 site
Luciferase
D
ns
E
12 x CSL-RE-LUC
12 x CSL-RE
β-Globin-min.

Figure 6

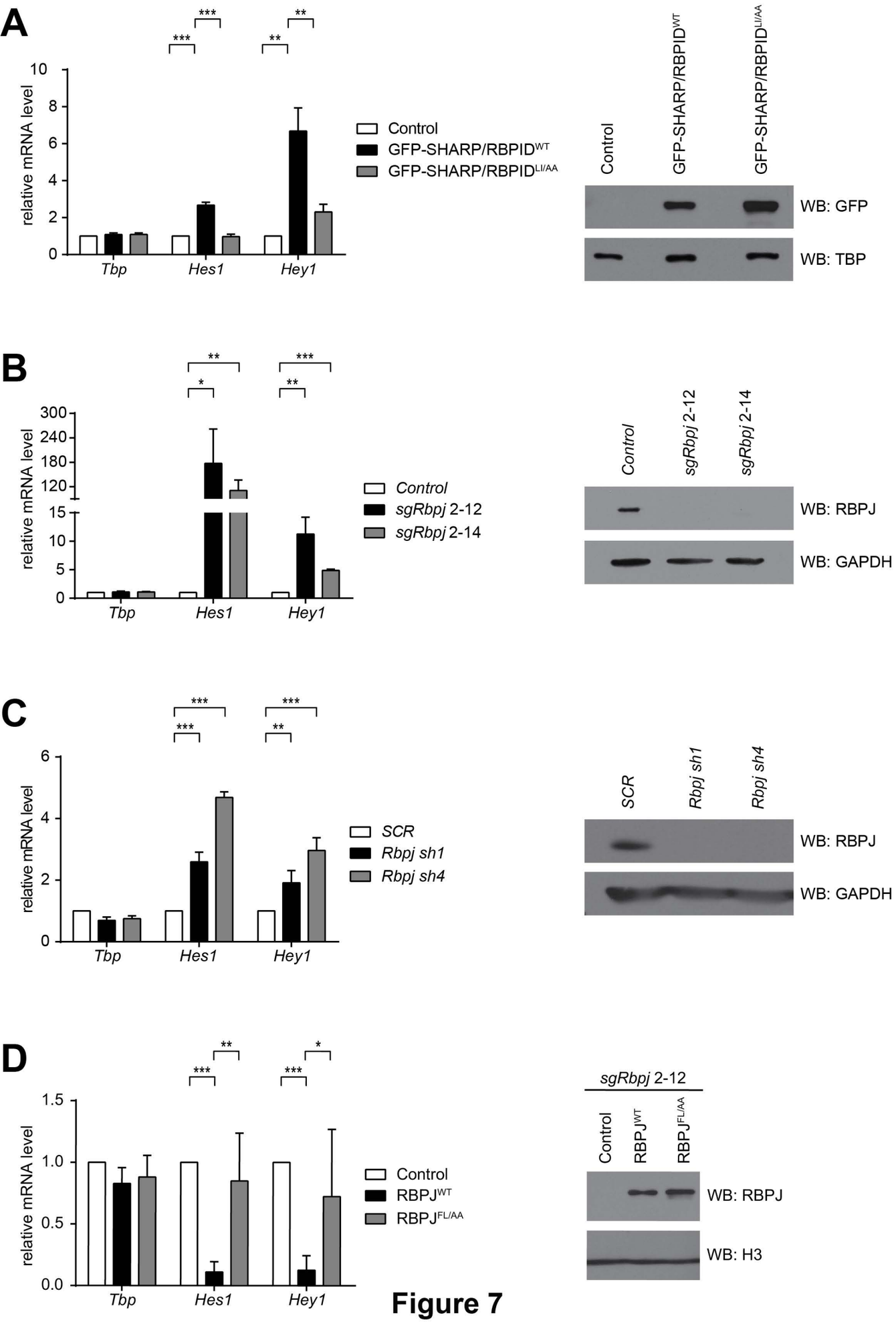
A
relative mRNA level
Control
GFP-SHARP/RBPID^WT
GFP-SHARP/RBPID^LI/AA
Tbp
Hes1
Hey1
WB: GFP
WB: TBP
B
Control
sgRbpj 2-12
sgRbpj 2-14
WB: RBPJ
WB: GAPDH
C
SCR
Rbpj sh1
Rbpj sh4
D
RBPJ^WT
RBPJ^FL/AA
WB: H3

Figure 7